

Design, Simulations, and Characterization of Self Powered Cantilever Based Piezoelectric Micro-Power Generator for Cardiac Pacemaker

Submitted in partial fulfillment of the requirements for the degree of

Master of Technology

in

VLSI Design

by

Hitesh Kumar Sharma

(Roll no: 2016Pev5091)

Under the guidance of

Dr. Dharmendra Boolchandani

Professor



Department of Electronics and Communication Engineering

MALAVIYA NATIONAL INSTITUTE OF TECHNOLOGY, JAIPUR 302017

June 2019



Department of Electronics and Communication Engineering
Malaviya National institute of Technology, Jaipur

Certificate

This is to certify that the dissertation report on “Design, Simulations, and Characterization of Cantilever Based Piezoelectric Micro-Power Generator for Cardiac Pacemaker” by *Hitesh Kumar Sharma* (2016PEV5091) is a bonafide work completed under my supervision, hence approved for submission in partial fulfillment for the Master of Technology in VLSI DESIGN, to the Department of Electronics and Communication Engineering, Malaviya National Institute of Technology, Jaipur during academic session 2018-2019 for the part time post graduation program of session 2016-2019. The work has been approved after plagiarism check as per institute rule.

Place: **Jaipur**

Date:

D. Boolchandani

Professor

Dept. of ECE

MNIT, Jaipur

ACKNOWLEDGMENTS

I am very grateful to my supervisor, Dr. D. Boolchandani, Professor for his constant guidance and encouragement and support to carry out this work. His excellent cooperation and suggestion provided me with an impetus to work and made the completion of work possible. He has been great source of inspiration to me, all through. I am very grateful to him for guiding me how to conduct research and how to clearly & effectively present the work done.

I would like to express my deepest sense of gratitude and humble regards to the Head of Department for providing necessary facility in the Department. I am also thankful to all other faculty members of ECE, MNIT for their valuable assistance and advice. I would also like to thanks to lab staffs, Ph.D. students and my friends for their support in discussions which proved valuable for me. I am indebted to my parents and family for their constant support, love, encouragement and sacrifices made by them so that I could grow up in a learning environment. Finally, I express my sincere thanks to all those who helped me directly or indirectly to complete this work successfully.

(Hitesh Kumar Sharma)

DECLARATION

I declare that,

1. The work contained in this dissertation is original and has been done by me under the guidance of my supervisor.
2. The work has not been submitted to any other Institute for any degree or diploma.
3. I have followed the guidelines provided by the Institute in preparing the dissertation.
4. I have conformed to the norms and guidelines given in the Ethical Code of Conduct of the Institute.
5. Whenever I have used materials (data, theoretical analysis, figures, and text) from other sources, I have given due credit to them by citing them in the text of the dissertation and giving their details in the references. Further, I have taken permission from the copyright owners of the sources, whenever necessary.

Hitesh Kumar Sharma
(2016PEV5091)

ABBREVIATIONS

PMPG	Piezoelectric micro power generator
MEMS	Micro-Electro Mechanical System
FESEM	Field Emission Scanning Electron Microscope
AFM	Atomic Force Microscope
DOF	Degree of Freedom
TMAH	Tetra Methyl Ammonium Hydroxide
ZnO	Zinc Oxide
PZT	Lead ZirconateTitanate
IGE	Inter Digital Electrode

ABSTRACT

This thesis describes about the design concept of piezoelectric micro power generator (PMPG) for the application of cardiac pacemaker. In cardiac pacemaker, the use of lithium iodide battery is replaced by piezoelectric power generator, which converts mechanical vibrations into electrical energy. In this thesis, we represent the design, simulations and characterization of PMPG cardiac pacemaker in the frequency range of 1 – 1.5 Hz and optimized the structure for 1.2Hz that is equivalent to human heart beat of 72 BPM using COMSOL Multiphysics. Taguchi orthogonal array method is used to validate the optimum design by varying eight control parameters as proof mass width, proof mass length, proof mass width, piezoelectric material, piezoelectric layer thickness, piezoelectric layer width, piezoelectric layer length, and silicon nitride thickness. L_{18} orthogonal array design is used to choose the most controlled variables or dimensions that can harvest the maximum amount of energy at frequency of 1.2 Hz.

Pacemaker requires small amount of power to start an operation. The source of this power is lithium iodide batteries, which takes about 2/3 of the total size of the pacemaker. Due to this, the size of typical pacemakers is about 42 mm, 51 mm, 6mm. By using the PMPG, this device size can be controlled to approximately 31 mm, and 20 mm in X and Y axis. The use of MEMS piezoelectric energy harvester for cardiac pacemaker has several advantages over traditional lithium iodide batteries which include short life time used for pulse generator, surgical costs will significantly diminish from using this device in cardiac pacemakers. Also, the patient's pain and tissue injury during the medical operation would be eliminated.

In this thesis, electro-deposition of copper and nickel are also done with the help of deposition set up by using the commercially available solvent of copper sulfate and nickel sulphamate respectively to choose the optimal material as a proof mass. For the experimental conclusion, a surface characterization is performed to view the surface morphology to select an optimal proof mass which is responsible for the low Eigen frequency at 1.2 Hz for cardiac pacemakers. The Bruker multimode 8 Atomic Force Microscopy (AFM) in tapping mode is used to identify the morphology of deposited Cu and Ni surface. 2D and 3D height images of AFM confirm that Cu deposition has some kind of porous and asymmetric shape structure with very high roughness of 200nm, whereas Ni has a circular shaped structure with very dominant roughness of 100 nm. This porosity and shape is also confirmed by Field Emission Scanning Electron Microscope (FESEM). A Nova NanoSEM 450 is used to clarify the morphology picture of both deposited films. FESEM images of Ni shows that the distribution of particle is in circular and ball shape structure while the Cu deposition indicates porosity and non-uniformity in the structure which makes it unsuitable for proof mass layer.

TABLE OF CONTENTS

Certificate	i
Acknowledgements	ii
Declaration	iii
Abbreviations	iv
Abstract	v
List of figures	x
List of Table	xiii
1. Introduction	
1.1. Thesis Organization	2
1.2. Research Objective	3
1.3. MEMS Sensors	3
2. Background	
2.1. Mechanical Sensors	6
2.2. MEMS Energy Harvesters	9
2.3. History of the Pacemakers	13
2.4. Advantage of Cardiac Pacemakers	14

3. Design and Simulation Results

3.1. Design and Simulations of cardiac pacemakers	17
3.1.1. Lumped and schematic of PMPG	17
3.1.2. Eigen Frequency Analysis	18
3.1.3. Frequency Domain Analysis	23
3.1.4. Taguchi Method	27
3.1.5. Designing of Experiment Using Taguchi Method	
3.1.5.1 Selection of Independent Variable	30
3.1.5.2 Selection of number of level settings for each independent variable	30
3.1.5.3 Selection of an orthogonal array	30
3.1.5.4 Assigning independent variable to each coloum	31
3.1.5.5 Conducting the experiments	31
3.1.5.6 Analyzing the data	32
3.1.5.7 Inference	32
3.1.6. Taguchi Implementation on MEMS PMPG	34
3.1.7. Damping in MEMS PMPG	37
3.1.8. Squeeze Film Damping	37

3.1.9. Slide Film Damping	38
3.1.10. Torsional Film Damping	39
3.2. Simulation Results	40
4. Deposition and Characterization	
4.1. Elctro-Deposition of Cu and Ni	42
4.2. Characterization of Deposited Films	43
5. Conclusion and Future Work	
5.1 Conclusion	44
5.2 Future Work	45
References	

LIST OF FIGURES

1.1 Basic elements of MEMS

2.1 Parallel plate capacitor, (b) represents the variable gap parallel plate capacitor, and (c) shows the variable area parallel plate capacitor.

2.2 Suspended proof (a) and (b) shows the implantation of conventional pacemaker with lithium iodide battery as a power source [5].

2.3 Lithium batteries performance over a time period [3].

2.4 (a) Electrode configurations of D_{31} and D_{33} mode for a cantilever beam, and (b) The parallel plate capacitor D_{31} mode and interdigitated electrode of D_{33} mode [5].

2.5 (a) And (b) shows the implantation of conventional pacemaker with lithium iodide battery as a power source [4].

2.6 History of pacemakers.

3.1 (a) Cantilever beam with tip mass, (b) Equivalent Lumped spring-mass model, and (c) Schematic of PMPG

3.2 (a) z axis displacement at frequency 1.2 Hz, (b) displacement of cantilever at atmospheric pressure, (c), (d) and (e) represents the undesired mode of oscillations at different frequencies.

3.3 (a) The generated electric potential at frequency of 1.2 Hz with maximum displacement., (b) shows the generated electric potential at constant pressure, and (c) represents the arrow surface distribution of electric potential verses ground potential.

3.4 (a) The generated electric voltage at frequency of 0.5 – 2 Hz, (b) shows the generated electric current across the resister of 100 Kilo ohm.

3.5 (a) The generated electric energy at frequency of 0.5 – 2 Hz, (b) shows the generated electric energy density across the resister of 100 kilo ohm.

3.6 The squeeze film damping air flow.

3.7 The slide film damping air flow.

3.8 The torsional film damping air flow.

3.9 The damping coefficient of squeeze film damping and (b) shows the damping coefficient of slide film damping at 1.2 Hz frequency.

4.1 (a), and (b) shows the FESEM images of electroplated Ni material on Si substrate.

4.2 The FESEM images of Cu electroplating at 25000 and 50000 magnification respectively.

4.3 The AFM 2D and 3D images respectively of electroplated Ni at 2 μm scale.

4.4 The AFM image of 2D and 3D respectively of electrodeposited Cu at 5 μ m scale.

4.5 (a) The roughness of electroplated Ni is $R_{\max} = 86.4$ nm, while (b) shows the roughness of electroplated Cu is $R_{\max} = 746$ nm.

LIST OF TABLES

- 2.1** Comparison between the d33 and d31 modes for energy harvesters.
- 3.1** The Eigen frequency of different proof mass.
- 3.2** The various dimensions used for each specified proof mass.
- 3.3** The L₉ orthogonal array design using the Taguchi method.
- 3.4** The 18 experiments corresponding to the L18 orthogonal array with respect to 8 variables.
- 3.5** The PMPG parameters level with respect to materials properties.
- 3.6** The generated electrical energy density with respect to the eigen frequency at all 18 experiments by Taguchi L18 orthogonal array.
- 3.7** Damping coefficient of squeeze and slide film damping.

CHAPTER 1: INTRODUCTION

1.1: Thesis organization

1.2: Research objective

1.3: MEMS sensors

CHAPTER 2: BACKGROUND

2.1: Mechanical sensors

2.2: MEMS energy harvesters

2.3: History of the pacemakers

2.4: Advantages of MEMS cardiac pacemakers

CHAPTER 3: DESIGN AND SIMULATION RESULTS

3.1: Design and simulation results of cardiac pacemakers

CHAPTER 4: DEPOSITION AND CHARACTERIZATION

4.1: Electro-deposition of Cu and Ni

4.2: Characterization of the deposited film

CHAPTER 5: CONCLUSION AND FUTURE WORK

5.1: Conclusion

5.2: Future work

CHAPTER-1

INTRODUCTION

1.1 Thesis Organisation

CHAPTER 1 Introduce thesis organization and its representation, objectives, and a brief description of MEMS.

CHAPTER 2 Introduce the MEMS Devices and the energy harvesters, the literature survey of the energy harvesters, history of the pacemakers, a brief description about cardiac pacemakers, and study of D_{31} and D_{33} mode with the advantage of D_{33} mode.

CHAPTER 3 Presents the design and simulation of MEMS cardiac pacemakers with the help of simulation tool COMSOL Multiphysics 5.1 and Coventor ware 14.

CHAPTER 4 Represents the electro-deposition of Copper and Nickel layer used in the proof mass and their characterization using FESEM and AFM.

CHAPTER 5 Presents conclusion and future scope of the MEMS micro power generator.

References

1.2 Research Objective

The primary objective of this research work is to design a MEMS piezoelectric energy harvester for the application of cardiac pacemaker using COMSOL 5.1 (Finite Element Method). Parameters are optimized according to structure resonant frequency at which, maximum displacement and energy are achieved, which is the most critical factor for the development of MEMS piezoelectric energy harvester. Copper and nickel material is optimized here for a selection of efficient proof mass. The main objectives are:

- To Optimize the Parameters according to the resonant frequency of the structure.
- To analysis frequency response and optimize the maximum energy to be harvested.
- To Design and simulate MEMS piezoelectric cardiac pacemakers using COMSOL 5.1.
- To perform Characterization of copper and nickel proof mass layer by FESEM and AFM.

1.3 MEMS Sensors

Micro-Electro-Mechanical Systems, or MEMS, is defined as a technology that can be used as miniaturized mechanical and electro-mechanical elements which are made using the techniques of micro fabrication. The dimensions of MEMS devices can be between 1 micron on the lower end of the dimensional graph, all the way to several millimeters. Also, the MEMS devices can vary from quite simple structures having no moving elements, to complex electromechanical systems with multiple moving parts with several degrees of freedom (DOF) under the control flow of integrated microelectronics. The one primary useful

term of MEMS devices is that there are at least a few elements having some sort of mechanical functionality either these elements can move or not. The term used to define MEMS can vary in different parts. In the US, they are generally called MEMS, while in some other area of the world, they are called “Microsystems Technology” or “micromachined devices” [1].

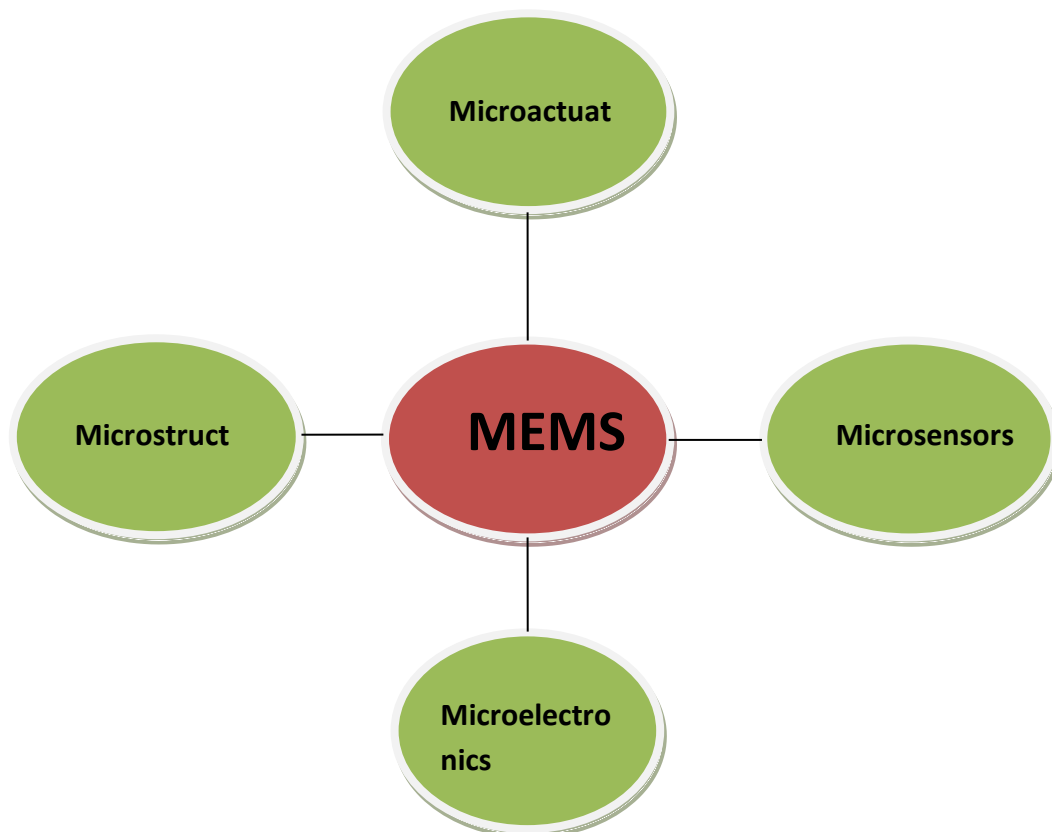


Fig 1.1. Basic elements of MEMS

In the most general ways, MEMS term consists of mechanical microstructures, microsensors, microactuators and microelectronics, all integrated onto the single silicon chip. This is shown in schematically in figure 1.1. Microsensors and microactuators are considered as the transducers which generally convert the one energy form to another. Microactuators converts the electrical signal into the mechanical form while in the case of microsensors, this is vice versa.

MEMS energy harvesters is a device which has dimensions at microscale and capable of storing the energy that can be used in multiple application. MEMS-based piezoelectric energy harvester converts the mechanical vibrations into electrical energy and generates a useful electrical power that is useful in low power electronics devices for various applications as wireless applications, biomedical applications, energy storage devices etc.

Chapter 2

BACKGROUND

2.1 Mechanical Sensors:

In MEMS, various type of sensors is used depending upon their mode of principal and sensing mechanism. These are categorized as capacitive, piezoelectric, and piezoresistive.

(A) Capacitive Sensors:

Capacitive sensors are defined as the sensors, which generate the output by sensing the change in capacitance phenomenon. This is widely used in the MEMS and based on the parallel plate capacitor in which one conducting plate is fixed, and another plate is movable. By this movable conducting plate, there is a change in capacitance by acting variable area or variable gap action.

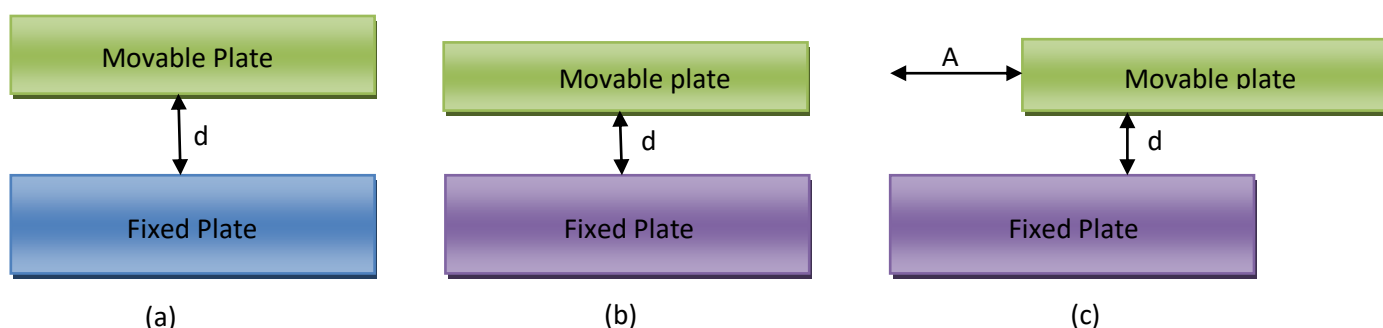


Fig. 2.1 (a) represents the parallel plate capacitor, (b) represents the variable gap cparallel plate capacitor, and (c) shows the variable area parallel plate capacitor.

(B) Piezoresistive sensors:

Piezoresistive sensors are the sensors in which when we apply the strain or stress; then there is a change in resistance in the sensors that is proportional to the change in strain due to variation in device dimensions. Piezoresistive sensors are widely used in pressure sensors and fabricated by using bulk

micromachining process. In the bulk micromachining process, TMAH (Tetramethyl Ammonium hydroxide) is used to create a cavity in n or p-type substrate. This is highly used in semiconductors instead of metals.

(C) Piezoelectric Sensors:

Piezoelectric sensors are being more prevalent in current MEMS fabrication because of ease to fabrication, more straightforward structure, and a variety of applications. The essential dominating factor in this type of sensors is piezoelectric materials, which are responsible for generating the output power. This type of sensors is based on the piezoelectric effect in which force (stress) is applied on the one side of piezo material, and the electrical voltage is generated on the other side and vice versa. The various type of piezoelectric materials are defined as zinc oxide (ZnO), lead zirconate titanate (PbTiO₃), PZT 5A, quartz, etc. PZT is mostly used in MEMS applications.

This type of sensors can be operated in both mode D_{31} and D_{33} mode depending upon the applications.

(D) Resonant Sensors:

In MEMS, The resonant structure is designed for vibrating at their Eigen or resonance frequency. All these can be attached to membranes/diaphragm or designed to adhere to a particular substance. Movement of the membrane or increased build-up of the binding element will affect the resonant frequency and can be monitored using implanted piezoresistors.

Types of the mechanical sensor include:

- **Strain Gauge** - A strain gauge is a conductor or semiconductor which is designed on or bonded directly to the surface to be measured. For an example of a polysilicon strain sensor unable to be fabricated by conventional method then

MEMS is an implantable piezoresistive strain gauge to measure forces in heart and brain tissue.

- **Accelerometer** - Accelerometers are the sensors which are used to sense acceleration by using a suspended proof mass on which external acceleration can act (Figure 2.2). By acceleration (or deceleration), a force ($F=ma$) is generated on the proof mass which causes a displacement in proof mass. The force or displacement is calculated by piezoresistive and capacitive effects.

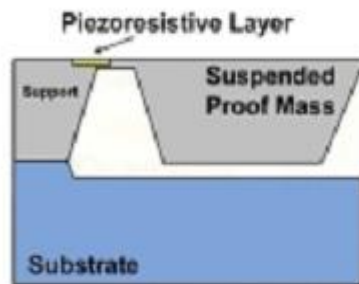


Fig 2.2. Suspended proof mass in a piezoresistive accelerometer [2]

- **Gyroscope** - A gyroscope is a sensor that measures the rate of rotation of an object and detects inertial angular motion. The applications involved as in space, missile navigations, etc. This is based on the Coriolis force on a body in a rotating frame. MEMS gyroscopes use vibrating structures with proof mass because of the difficulty of micromachining rotating parts with sufficient useful mass and resonance frequency is controlled by proof mass.
- **Pressure Sensors**- MEMS pressure sensors are generally based on thin membranes with sealed gas or vacuum-filled cavities on one side of the membrane and the pressure to be measured on the other side. Piezoresistive and capacitive membrane deflection measurement techniques are the most commonly used in commercial pressure sensors[2].

2.2 MEMS Energy Harvester:

MEMS energy harvester is a device which stores the energy generated from mechanical sources. In recent years, energy harvesting is attracted because of the limited battery life, dimension issue, used in the mobile and biomedical applications. MEMS Piezoelectric energy harvesters are the main component of such type of system. Solar power is also one of the sources of energy harvesting, but its use is limited in the dark field. That's why piezoelectric energy harvesters are playing a rigid role in the current scenario. Various ambient energy sources, such as solar, thermal, acoustic, and mechanical energies, have been investigated for micro-power generating devices. The potential energy sources should have high power density with long lifetimes (wireless sensors have a 10-year lifetime) and low product cost in micron size. Solar energy and mechanical vibration were considered, and their estimated power density and lifetime are compared with the conventional chemical batteries as shown in figure 2.3 [3]

MEMS piezoelectric energy harvesters store the energy when some mechanical vibrations is applied to at one end of the piezo materials, and the electric voltage is generated at the other end. Various piezo materials have significant properties to generate electrical energy as lead zirconate titanate (PZT), PZT 5A, PZT 5B, ZnO, BaTiO₃, etc. There are two prominent modes used in piezo electric micro power generator (PMPG) to generate power. These are denoted as D_{31} and D_{33} mode.

High conversion efficiency is a prime issue for piezoelectric energy harvesters in current technology. Based on robust surface micromachined fabrication technology, the single cantilever is designed to develop the piezoelectric MEMS energy harvester by ambient vibration sources. The shape of the cantilever is varied to improve the power density by distributing the strain on the piezoelectric film.

Besides the improvement of power density, the cantilever arrays are fabricated

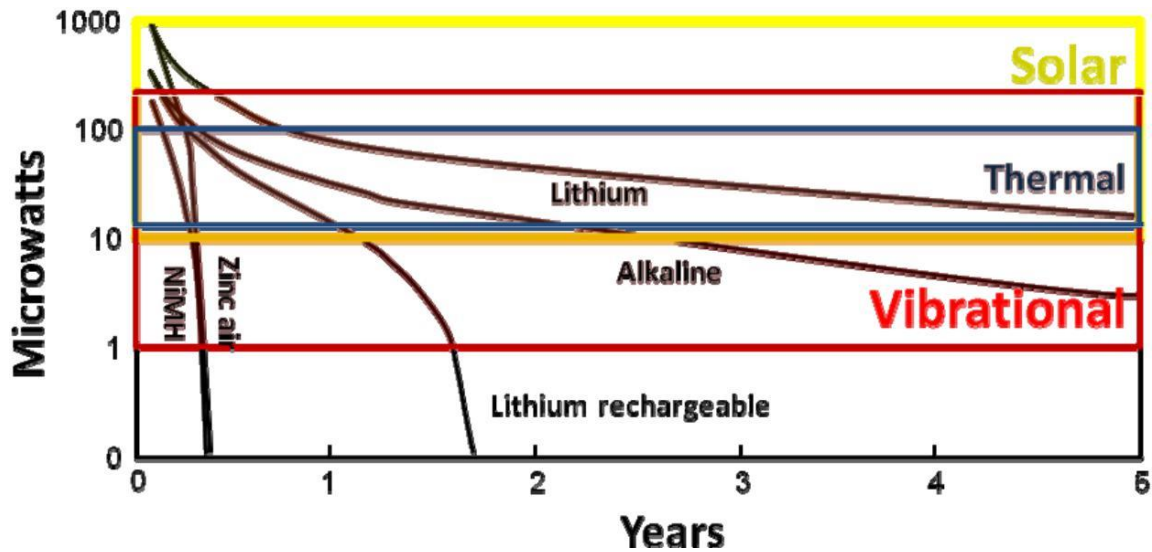


Fig. 2.3 represents lithium batteries performance over a time period [3]

to obtain high power and broadband working frequencies. The cantilever array design shows the feasibility of multiple cantilevers being integrated for a single application. The array device can be enabled by precise frequency control through advanced fabrication and design.

For the design and fabrication of the MEMS devices, Jeon et al. [4] have successfully developed the first MEMS-based micro power generator using the d_{33} mode of PZT material. A $170\mu\text{m} \times 260\mu\text{m}$ PZT beam has been fabricated. The maximum output power of $1.01\mu\text{W}$ across the load of $5.2\text{M}\Omega$ at its resonance frequency of 13.9 kHz has been observed. The corresponding energy density is $0.74\text{mWh}/\text{cm}^2$, which compares favorably to the values of lithium-ion batteries.

D_{31} mode is a mode in which external force or vibrations are applied in the x-direction, and the output voltage is generated in the z-direction or 3-direction.

In D_{33} mode, external vibration or forces are applied in the z-direction, and the output voltage is also measured in the z-direction, as shown in figure 2.4. In

PMPG, the D_{33} mode is preferred because of its ability to generate maximum power for the same dimensions, parameters, and materials as compared to D_{31} mode.

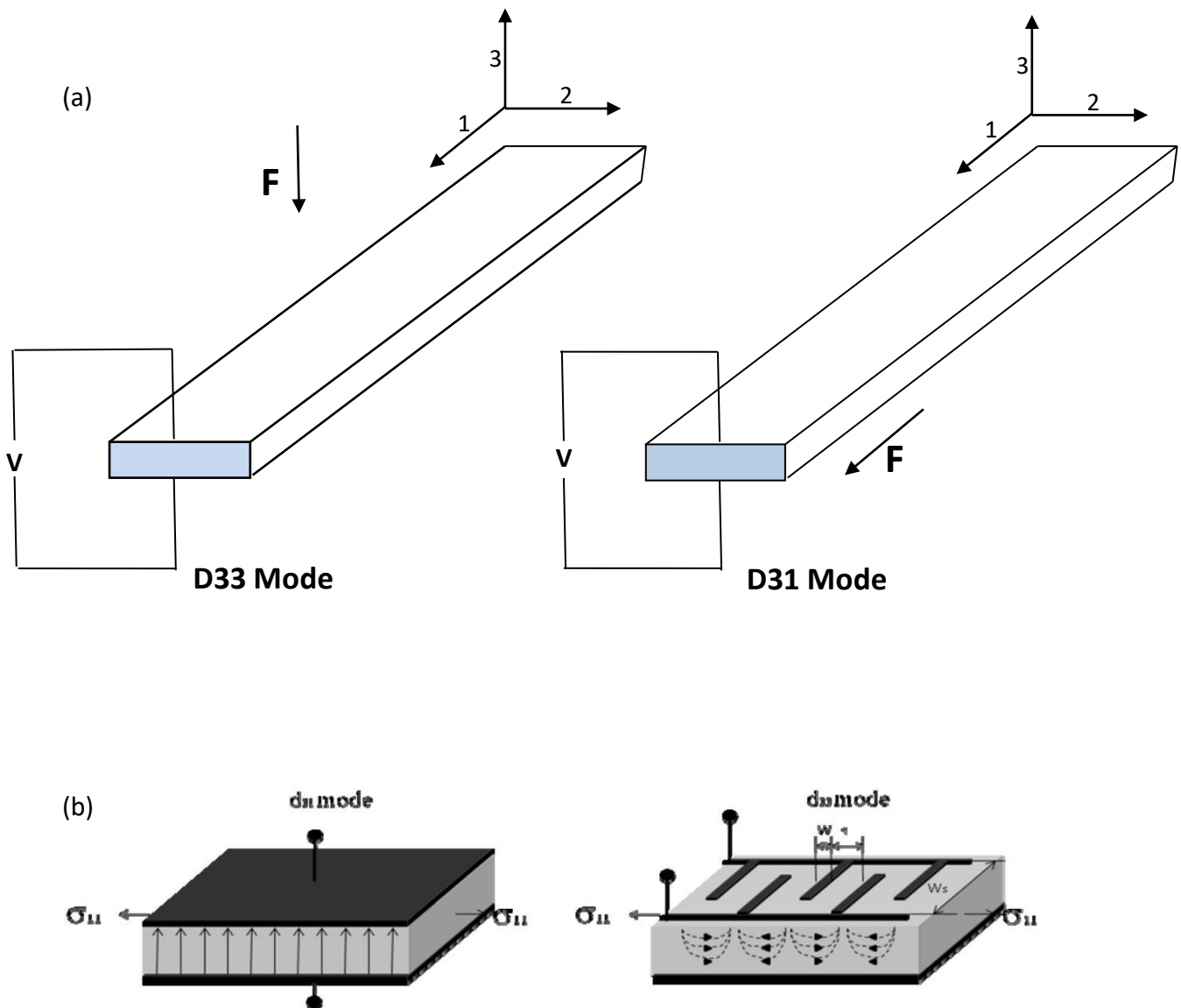


Fig. 2.4 (a) represents electrode configurations of d_{31} and d_{33} for a cantilever beam, and (b) indicates the parallel plate capacitor of D_{31} mode and interdigitated electrode of D_{33} mode [5].

The D_{31} approach uses top and bottom electrode concepts in energy harvesters while the interdigital electrodes (IGE) are used in the D_{33} mode to increase the sensitivity. The fabrication of electrode in D_{31} mode is more accessible than D_{33} mode that's why D_{31} mode is more superior to produce a tremendous amount of current while D_{33} mode is responsible for large voltage generation.

To draw the constitutive equation for D_{31} mode, let assume l_b is the length of the beam, l_m is the length of proof mass, h_p is the thickness of piezoelectric material, h_s is the thickness of beam material (silicon), w_b is the width of beam, z is the vertical base displacement, and y is the distance to neutral axis of beam.

The constitutive equation of piezoelectric materials is defined as:

$$T_p = C_{pq}^E S_q - e_{kp} E_k \quad (1)$$

$$D_i = e_{iq} S_q + \varepsilon_{ik}^S E_k \quad (2)$$

where T is the stress (N/m²), S the strain, E the electric field (V/m), D is the electric displacement (Coulomb/m²). “ C^E ” is the stiffness measured under the constant electric field. “ ε^S ” is the dielectric constant or permittivity under constant strain. “ e ” is the piezoelectric constant (Coulomb/m²).

Some other forms of the constitutive equations are:

$$S_q = S_{pq}^E T_p + d_{kq} E_k \quad (3)$$

$$D_i = d_{ip} T_p + \varepsilon_{ik}^T E_k \quad (4)$$

$$S_q = s_{pq}^D T_p + g_{kq} D_k \quad (5)$$

$$E_i = -g_{ip} T_p + \beta_{ik}^T D_k \quad (6)$$

$$T_p = c_{pq}^D S_q - h_{kp} D_k \quad (7)$$

$$E_i = -h_{iq} S_q + \beta_{ik}^S D_k \quad (8)$$

Equation 1 and 2 can be written in matrix form as:

$$\begin{Bmatrix} T \\ D \end{Bmatrix} = \begin{bmatrix} c^E & -e \\ e & \varepsilon^S \end{bmatrix} \begin{Bmatrix} S \\ E \end{Bmatrix} \quad (9)$$

So the optimized power in D_{31} and D_{33} mode is:

$$|P_{opt}| \approx \frac{(F_B \ddot{z}_B)^2}{16\sqrt{MK\varepsilon_m}} \quad (10)$$

Table 2.1 Comparison between the d_{33} and d_{31} modes for energy harvesters.

	d_{33}	d_{31}
Pro	<ul style="list-style-type: none"> - High dielectric constant - Easy output voltage regulation 	<ul style="list-style-type: none"> - Large charge density - Easy control of PZT microstructure o
Cont.	<ul style="list-style-type: none"> - High % loss factor (wasted area under electrode) - Requires optimization of IDE - Complicated modeling due to IDE 	<ul style="list-style-type: none"> - Low dielectric constant

2.3 History of pacemakers:

A pacemaker is a small device that placed in a human body either near chest or abdominal, to help to control abnormal heart beats. This device creates an electrical pulse so that the heart could beat at a regular rate. The usual range of human heart beat rate varies from 60 to 100 BPM (beats per minute) that is equivalent to 1-1.5 Hz. When heart rate below 60 or greater than 100, then it belongs to abnormal condition and pacemaker is required [1].

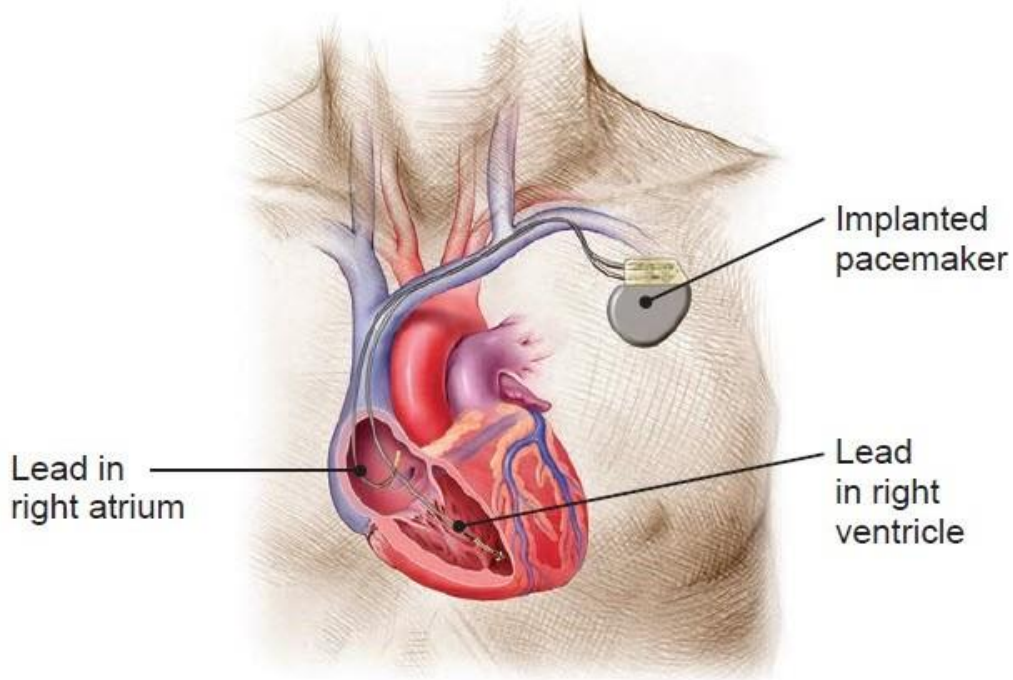
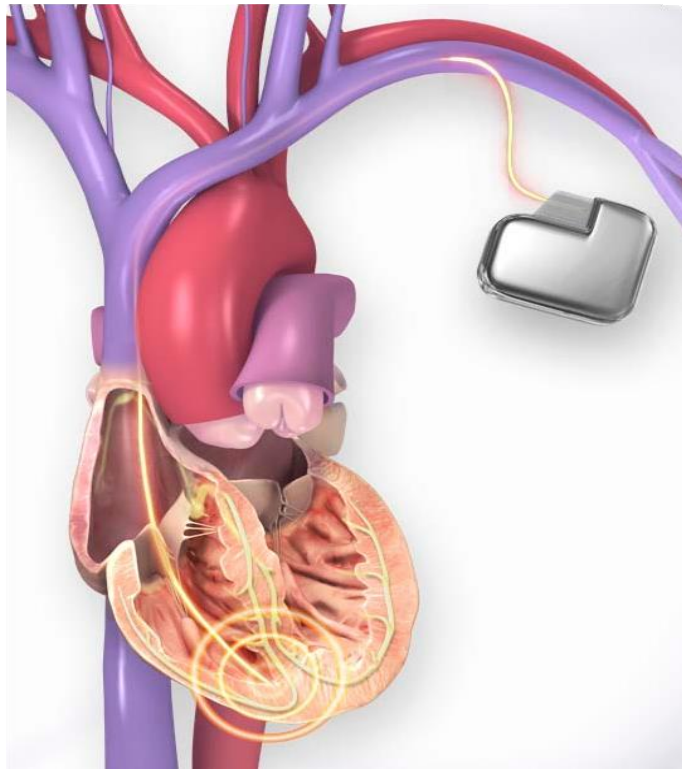


Fig 2.5 (a), and (b) shows the implantation of conventional pacemaker with lithium iodide battery as a power source [15].

The pacemaker consists of a battery, an electrical pulse generator, and the electrodes which are surrounded by a thin metal box. The battery powers the generator, and the electrode connects the generator to the heart. The heart

detects heart electrical activity and sends the signal to the generator that generates the pulses and controls the heart beats.

Lithium iodide battery is generally used to power electronic devices, and it has a short life span, and a **high ratio between mass and electrical power**: hazards and high replacement costs for those batteries, especially in medical implant applications. Removing of pacemakers after batter life is over, the replacement surgery may also be include swelling, bleeding, or infection in the area where they paced, blood vessel or nerve damage as well a collapsed lung. To overcome all these issues, motivated to develop power harvesting devices as PMPG (piezoelectric micro power generator). Due to low power requirements and small device dimensions, PMPG can supply enough power for a variety of applications, such as wireless sensor nodes, wrist watches, and biomedical implants.



Fi. 2.6 History of pacemakers

Piezoelectric micro-power generator (PMPG) converts mechanical vibration into electric energy through piezoelectric effects. In pacemakers, for the cardiac activities, the use of PMPG removes the use of a traditional lithium iodide

battery. PMPG can harvest the mechanical movement of the heart beat to be converted into usable electrical power in the frequency range of 1-1.5 Hz. Nowadays, artificial pacemakers are externally programmed and permit the patient to choose the operating mode for different activities. Human organ movement can generate power for mobile electronics. The energy content of the heart vibration spectrum given energy harvesting is found a mean power of 20 μW to the cardiac pacemaker at lower frequencies (15 – 30 Hz).

The pacemakers require a small amount of power to start an operation. The source of this power is lithium iodide batteries, which takes about 2/3 of the total size of the pacemaker. Due to this, the size of a typical pacemakers is about 42 mm, 51 mm, 6mm. By using the PMPG, this device size can be controlled to approximately 31 mm, and 20 mm in X and Y axis [1].

2.4 Advantage of MEMS pacemakers:

The main advantage to use PMPG is to solve the short lifetime of the traditional lithium iodine battery used for pulse generator in cardiac pacemakers. So the cost of replacement batteries will be eliminated by using such self-powered devices. Surgical costs will significantly diminish from using this device in cardiac pacemakers. Also, the patient's pain and tissue injury during the medical operation would be eliminated.

Chapter 3

DESIGN AND SIMULATION RESULTS

3.1 Design and simulation results of MEMS cardiac pacemaker:

A cantilever based MEMS piezoelectric micro power generator is simulated using COMSOL Multiphysics 5.1. Here a PMPG is designed, which can harvest the electrical energy which is generated by the mechanical movement of the heart beat in the frequency range of 1-1.5 Hz.

COMSOL Multiphysics is used to perform the eigen frequency analysis, and frequency response mode while the squeeze film and slide film damping are achieved by using Coventor ware tool. Eight control parameters are used, which are: piezoelectric material, proof mass material, proof mass thickness, proof mass length, piezoelectric layer thickness, piezoelectric layer width, silicon nitride layer thickness. Orthogonal array Taguchi method is used to find out the optimal design parameters. Taguchi method is performed for three levels, and 18 different simulations are performed to calculate the eigen frequency at 1.2 Hz, equivalent to 72 beats per minute. The maximum output power is observed at this frequency.

3.1.1 Lumped and schematic of PMPG:

The figures below show the cantilever beam with tip mass, equivalent spring mass damping model, and schematic of PMPG respectively in figure (a), (b), and (c).

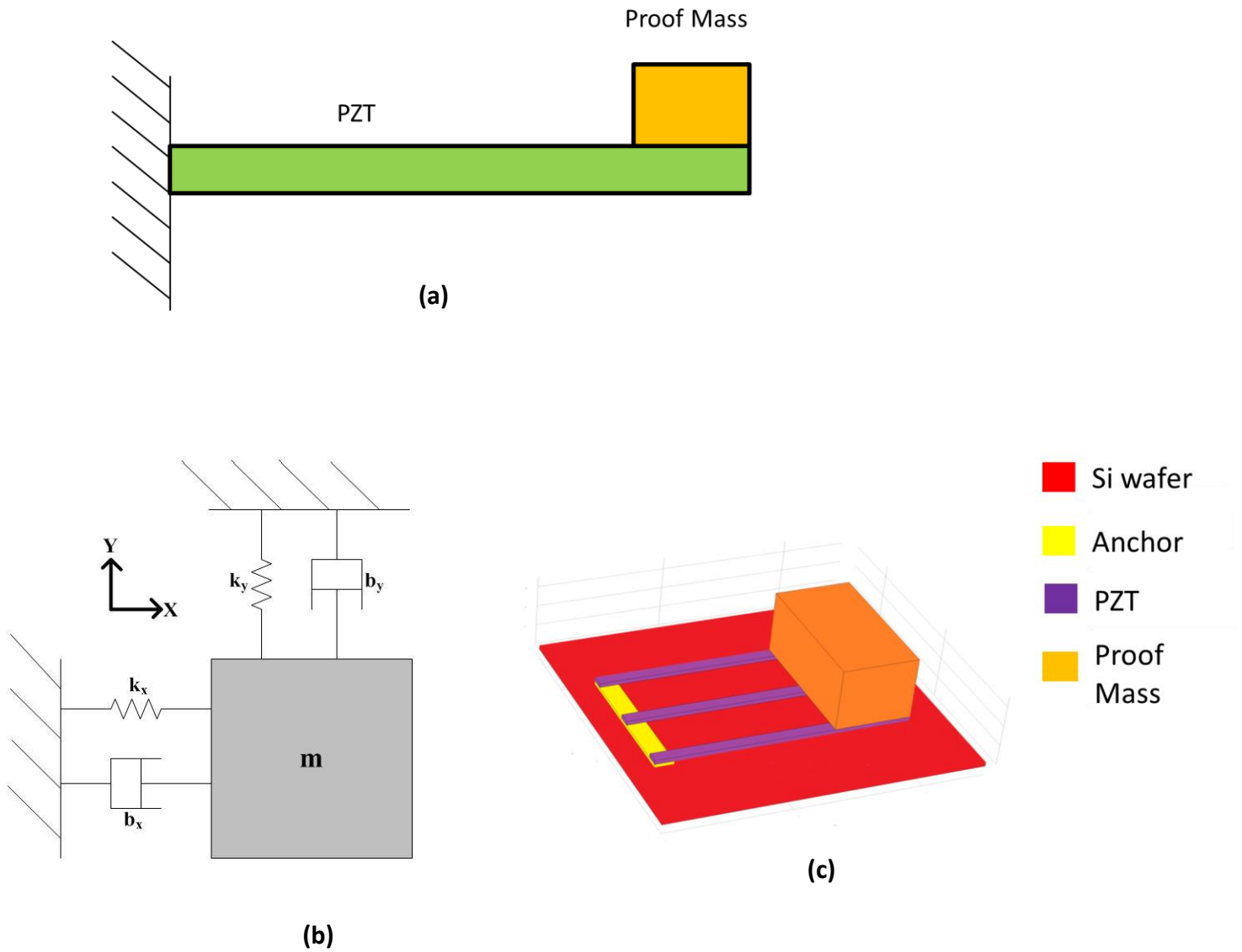


Fig 3.1 (a) Cantilever beam with tip mass, (b) Equivalent Lumped spring-mass model, and (c) Schematic of PMPG

3.1.2 Eigen frequency analysis:

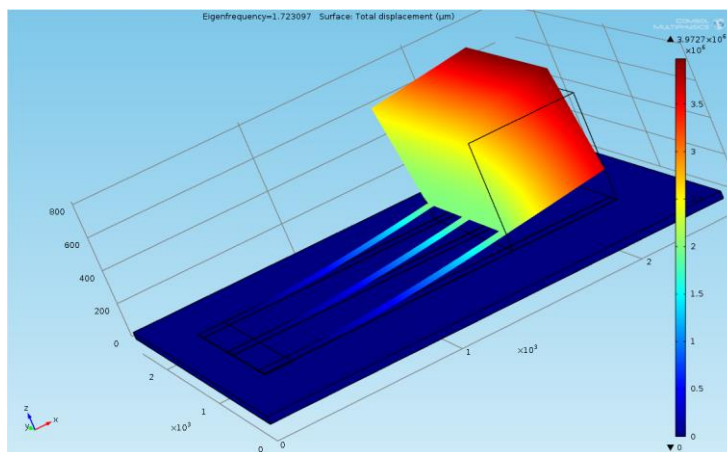
Eigen frequency analysis is responsible for the movement of the structure in possible directions. The eigen frequency analysis is done by COMSOL Multiphysics 5.1. Eigen frequency is calculated for every mode and correlated with the theoretical equation as [6]:

$$f = \frac{1}{2\pi} \sqrt{\frac{k}{m}} \quad (11)$$

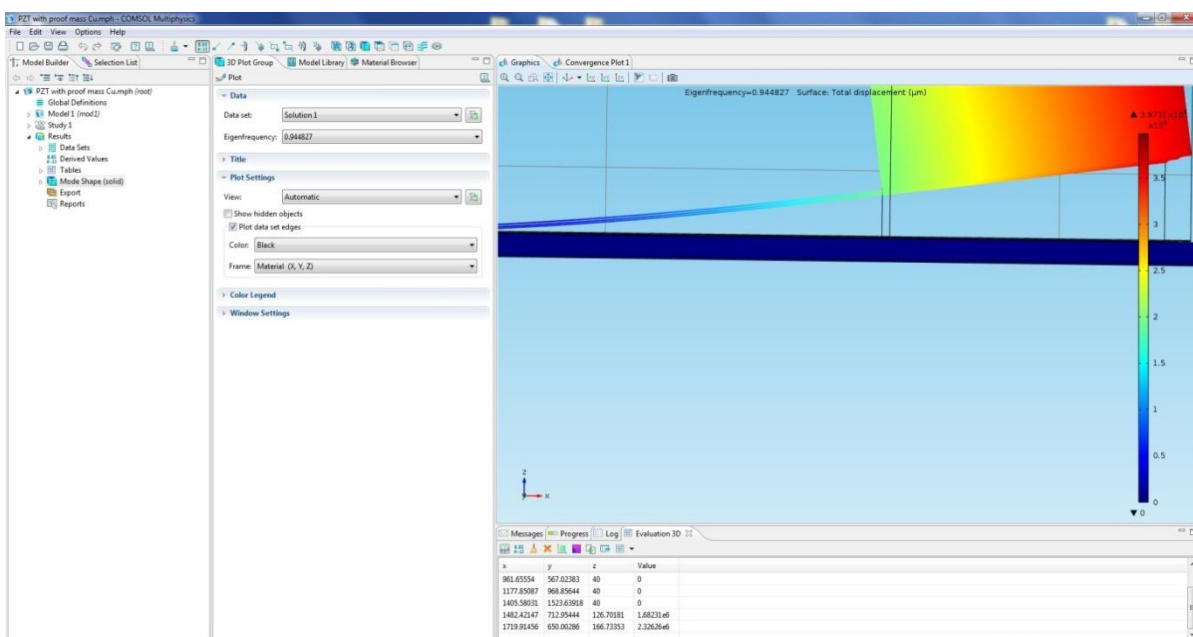
Here f = Eigen frequency, k = spring constant, m = total mass including proof mass. The proof mass is responsible for maintaining the resonance frequency. The resonance frequency can be achieved either by varying the stiffness or spring constant or proof mass.

The simulation is performed for six modes in which four modes are displayed here in figure 3.2. Every mode has its resonance frequency and movement in different directions. Some modes are undesirable; we are interested in the z-axis displacement mode, which can operate at only 1.2 Hz, which is equivalent to the human heart beat as shown in figure 3.2 (a) and (b).

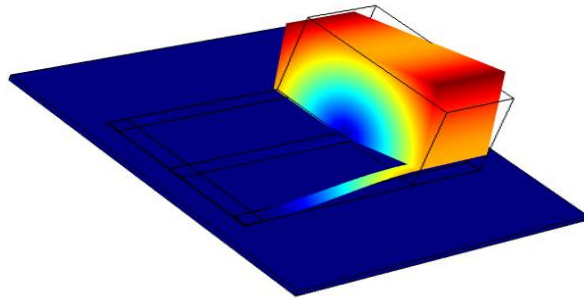
(a)



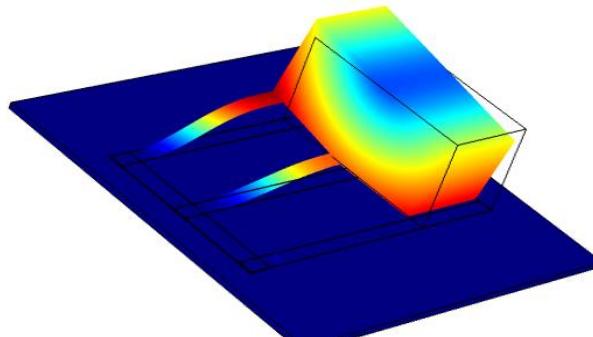
(b)



(c)



(d)



(e)

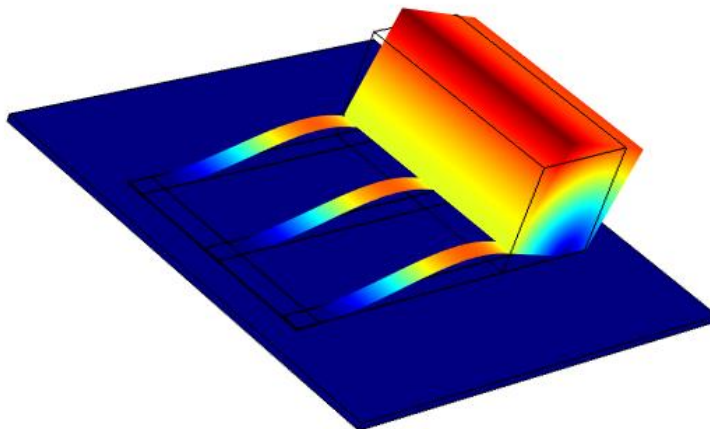


Fig. 3.2 (a) represents z axis displacement at frequency 1.2 Hz, (b) displacement of cantilever at atmospheric pressure, (c), (d) and (e) represents the undesired mode of oscillations at different frequencies [14].

PMPG is simulated as actuator mode, static parametric solver was used in COMSOL to find the deflection for the voltage range 0–20 V and shows the linear relationships between applied voltage at the bottom of piezoelectric layer while the top is grounded and the total displacement is at the center of Proof mass shown in fig. 3.2 (a). When zero volts are applied, the displacement at the center of the proof mass is about 25 μm . This simulation is performed on various materials used in proof mass as Nickel, Copper, PMMA, and Aluminium. The table 3.1 shows an experiment performed on various proof mass as well as their resonance frequency. Resonance frequency for the first four modes of operation is presented below in table 3.1. The maximum total displacement at the center of the proof mass for PMPG occurs at the first mode of operation at 1.16 Hz as shown in Fig. 3.2 (a) while the displacement at other mode is negligible; therefore maximum PMPG output power occurs at this mode. The first mode of simulation is required not only because of the maximum displacement but also the other modes do not show a uniform bending of cantilever beam as in z-direction. Therefore some parts of cantilever beam show compression while the other shows tension and causes charge cancellation along the cantilever beam, and degrades PMPG output power and its efficiency. The first mode of operation shows that 93 % of PMPG's total displacement and output power produced in the range of (1–1.5 Hz), so that PMPG can work probably when the heart rate is between 60–85 BPM and the maximum displacement is at 1.2 Hz (72 bpm). No displacement in the Y direction at the first mode Fig. 3.2 (a) while the displacement in the X direction is negligible compared with the Z direction, as shown in Fig 3.2 (b) respectively. The maximum displacement in the z-direction only.

Table 3.1 indicates the eigen frequency of different proof mass.

S. No.	Proof Mass	Eigen Frequency (Hz)
1	Aluminum	1.7
2	Copper	1.3
3	Nickel	1.16
4	PMMA	2.6

Table 3.1 indicates the resonance frequency analysis by using various proof mass and their corresponding eigen frequency. Table 3.2 suggests about the various parameters used during the simulations to estimate the resonance frequency.

As a result of simulations, it is concluded from table 3.1 that copper and nickel has a very close resonance frequency to cardiac pacemaker's resonance frequency of 1.2 Hz. But due to the higher mechanical strength, we used nickel as a proof mass to obtain further simulation results.

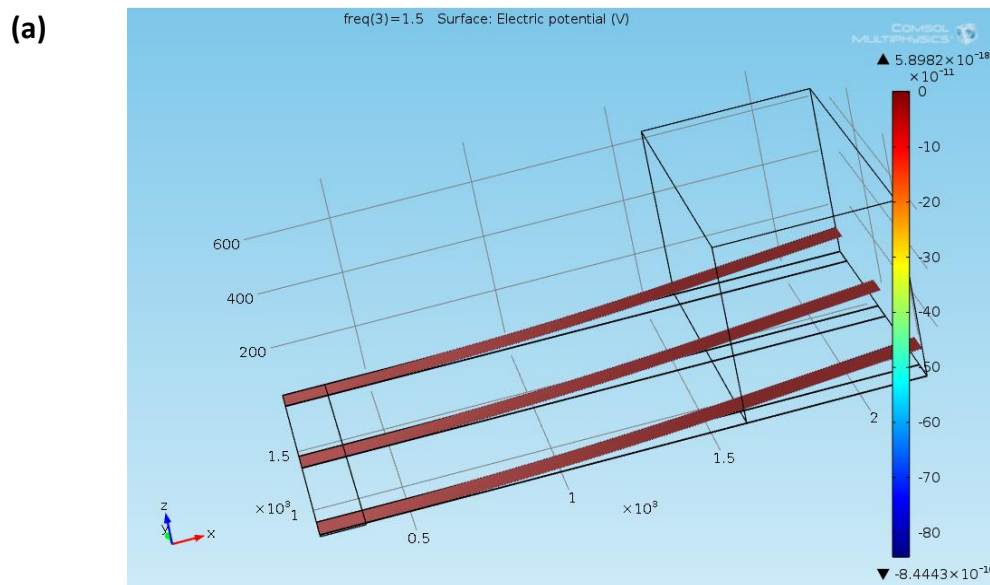
Table 3.2 describes the various dimensions used for each specified proof mass.

S. No.	Dimensions used	Al proof mass	Cu proof mass	Ni proof mass	PMMA proof mass
1	Proof mass thickness (μm)	600	600	600	600
2	Proof mass length (μm)	600	600	600	600
3	Proof mass width (μm)	1200	1200	1200	1200
4	Piezoelectric layer thickness (μm)	2	2	2	2
5	Piezoelectric layer width (μm)	100	100	100	100
6	Piezoelectric layer length (μm)	2000	2000	2000	2000
7	Piezoelectric material	PZT 5A	PZT 5A	PZT 5A	PZT 5A

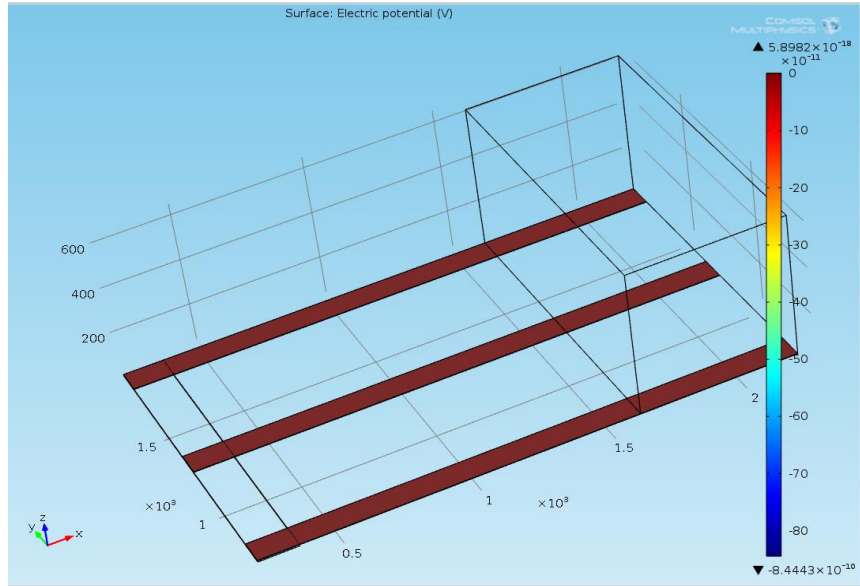
3.1.3 Frequency Domain Analysis:

The frequency domain analysis is performed on the Ni proof mass using the same dimension as in the eigen frequency analysis. The frequency range is varied from 0.5 Hz to 2 Hz, and the simulations are carried out. We set the current, voltage, power, and energy curve by using the frequency domain simulations at 1.2 Hz resonance frequency.

The output energy we achieved here is approximate $21 \mu\text{W}/\text{cm}^3$. The current, electric potential, power, and energy curves are also displayed in figure 3.4 and 3.5 with respect to frequency. The optimum electric energy density for proof mass material was obtained for Ni. Ni has signal to noise ratio of 10.55 [1] and it decreases upto 6.342, when the proof mass material is changed from nickel to some other high density materials. Therefore electric energy density and output power is also decreased because it increases the total mass which results in a huge change of PMPG resonance frequency from the required 1.2 Hz and hence lowers the output power. For the piezoelectric material, the optimum electric energy density is found for PZT5A piezo material. It generates large amount of output power due to the high piezoelectric coupling coefficient, especially at low-frequency applications.



(b)



(c)

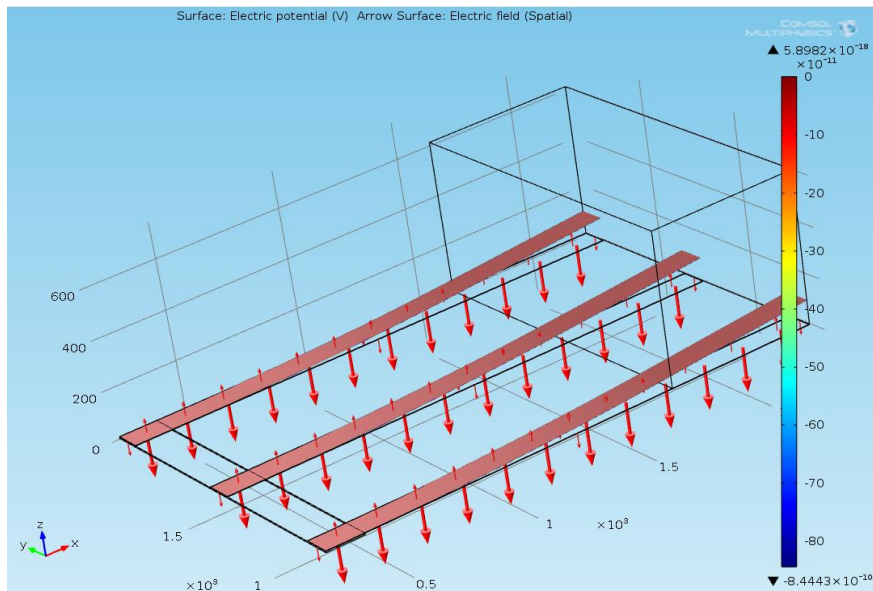


Fig 3.3 (a) represents the generated electric potential at frequency of 1.2 Hz with maximum displacement., (b) shows the generated electric potential at constant atmospheric pressure, and (c) represents the arrow surface distribution of electric potential verses ground potential [14].

The figures 3.3 (a), (b) represent the simulations of electric potential generated at frequency 1.2 Hz. Figure 3.3 (c) here represents the arrow indication of the generated electric field according to polarity. The electric potential is generated

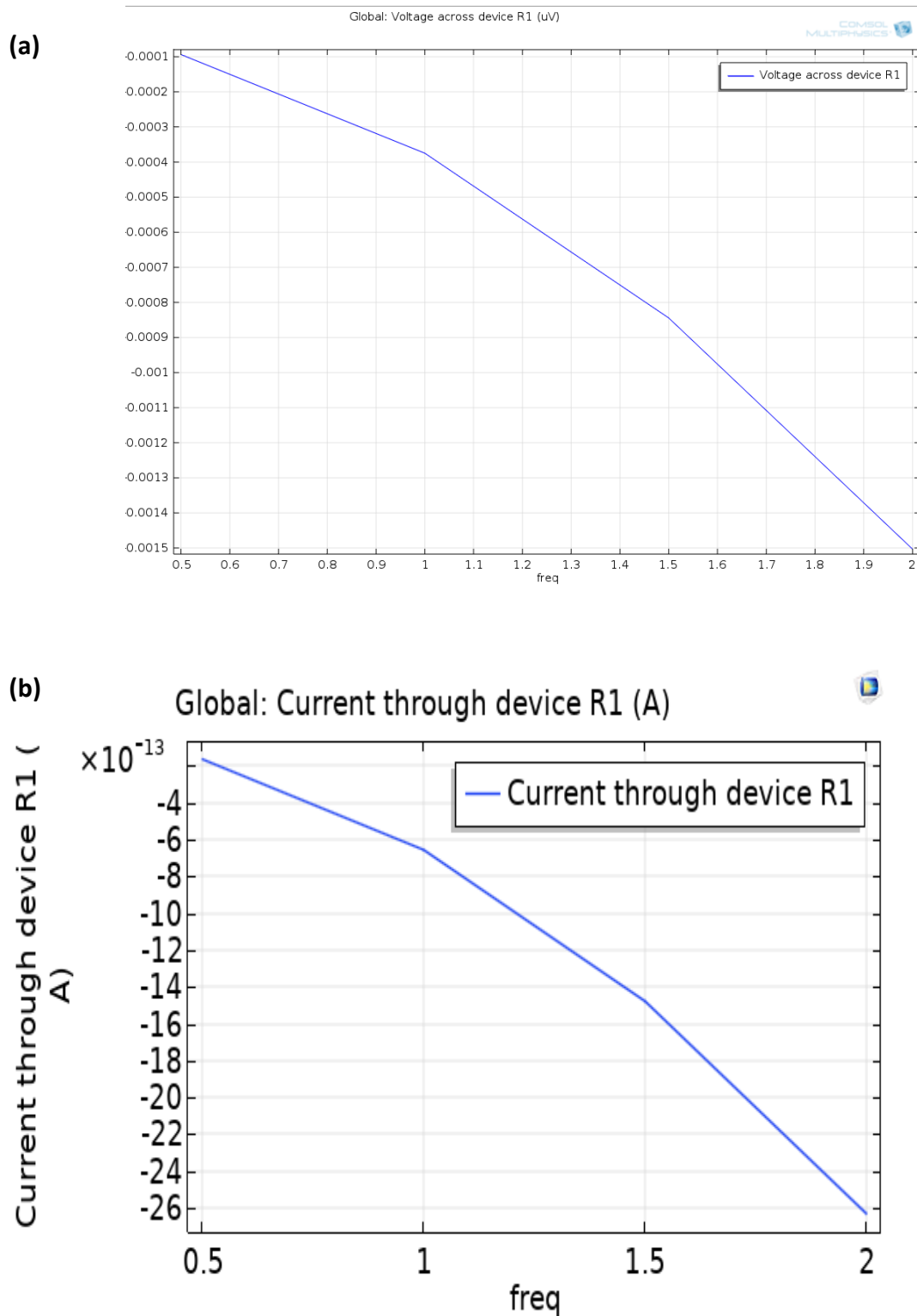


Fig. 3.4, (a) indicates the generated electric voltage at frequency of 0.5 – 2 Hz, (b) shows the generated electric current across the resistor of 100 Kilo ohm [14].

due to the displacement of structure in Z-direction.

The graph 3.4 (a) and (b) show the voltage and current with respect to the

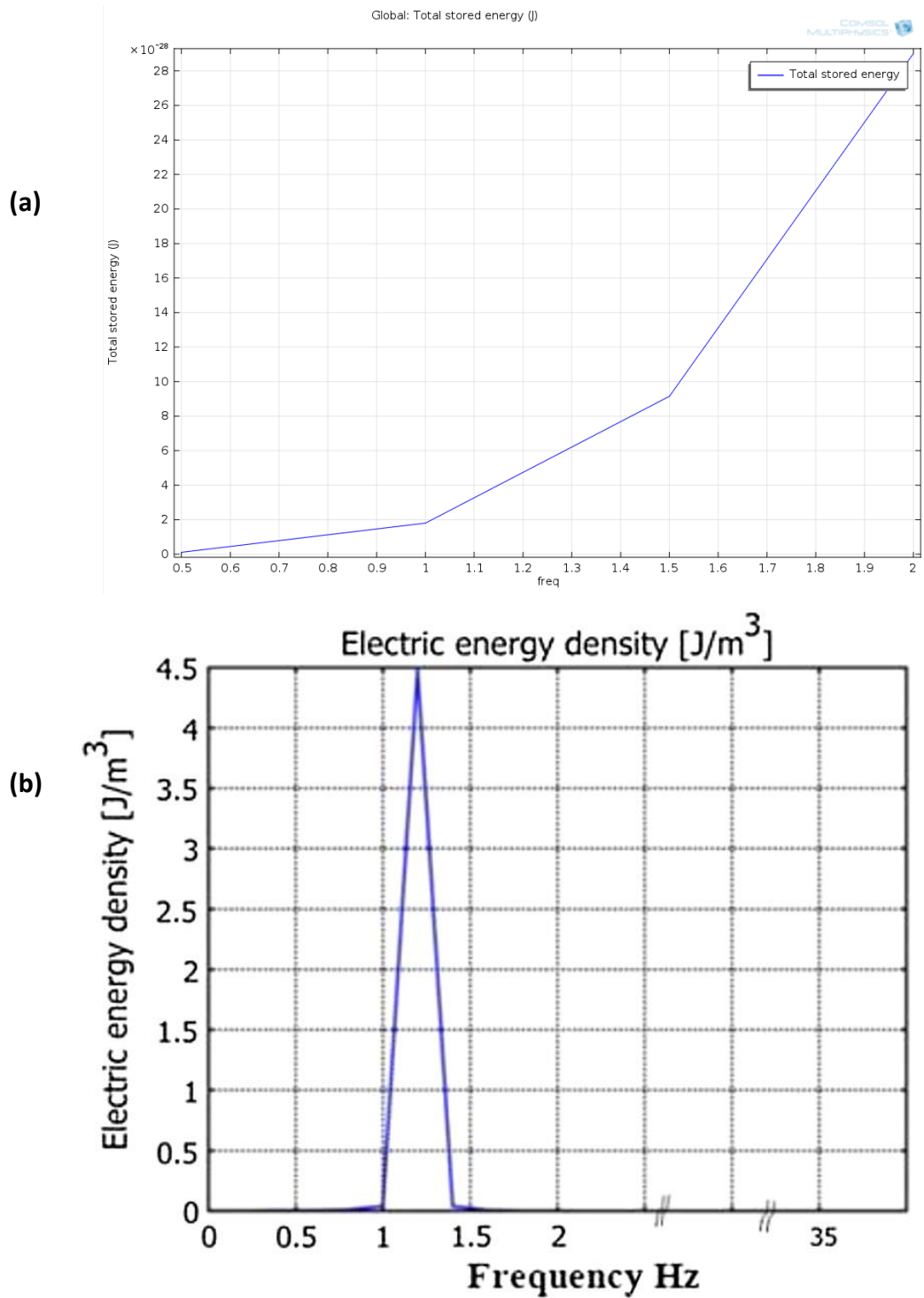


Fig. 3.5, (a) indicates the generated electric energy at frequency of 0.5 – 2 Hz, (b) shows the generated electric energy density across the resistor of 100 kilo ohm [14].

frequency range of 0.5 to 2 Hz and we achieved voltage and current at frequency 1.2 Hz are approximately 50 nV and .001 nA respectively and the figure 3.5 (a) and (b) show the stored energy with respect to eigen frequency, which is around 4.5×10^{-28} J . This energy is sufficient to operate the pacemaker at the frequency of 1.2 Hz. This energy can also be increased by varying the dimesions, appropriate choice of proof mass as well the piezoelectric material.

3.1.4 Taguchi Method:

Taguchi has investigated a new method of conducting the design of experiments which are based on well cleared guidelines. This method uses a special set of arrays called orthogonal arrays. These standard arrays stipulate the way of conducting the minimal number of experiments which could give the full information of all the factors that affect the performance parameter. The crux of the orthogonal arrays method lies in choosing the level combinations of the input design variables for each experiment [7].

Taguchi Method is based on an orthogonal array; it is used to find the most variable affecting power that harvests performance at a frequency range of 1-1.67 Hz. In our cardiac pacemaker design, there are eight variables which are proof mass material, piezoelectric material, proof mass length, proof mass thickness, piezoelectric layer width, piezoelectric layer thickness, silicon nitride thickness. Depending on these eight variables, we used L_{18} orthogonal array of taguchi method which described by the below formula:

The minimum number of experiments to be conducted is to be fixed based on the formula as [9]:

$$\mathbf{N\ Taguchi = 1+NV (L-1)}$$

Where NV = Number of parameter

L = Number of Levels

Here NV = 8, L =3; So N Taguchi = 17 (As 17 DOF)

When there are many standard orthogonal arrays available, each of the arrays is used for a specific number of independent design variables and levels . For example, if someone wants to conduct an experiment to understand the effect of 4 different independent variables with each variable having 3 set values (level values), then an L9 orthogonal array might be the used right choice. The L₉ orthogonal array is used for understanding the effect of 4 independent factors

Table 3.3 indicates the L₉ orthogonal array design using the Taguchi method

L ₉ (3 ⁴) Orthogonal array					
	Independent Variables				Performance Parameter Value
Experiments	Variable 1	Variable 2	Variable 3	Variable 4	
1	1	1	1	1	p1
2	1	2	2	2	p2
3	1	3	3	3	p3
4	2	1	2	3	p4
5	2	2	3	1	p5
6	2	3	1	2	p6
7	3	1	3	2	p7
8	3	2	1	3	p8
9	3	3	2	1	p9

each having 3 level values. This array assumes that there is no interaction between any two factors. While in many cases, no model assumption is valid,

there are some cases where there is a clear proof of interaction [8]. A typical case of interaction would be the interaction between the material properties and temp.

L18 orthogonal array is basically used to find the most affecting variable affecting the output power generated. In mathematics, in the field of combinatorial designs, an orthogonal array is a "table" (array) whose entries come from a fixed finite set of parameters (typically, $\{1,2,\dots,n\}$), arranged in such a way that there is an integer t so that for every selection of t columns of the table, all ordered t -tuples of the symbols, formed by taking the entries in each row restricted to these columns, appear the same number of times. The entity t is called the strength of the orthogonal array. Here is a simple example of an orthogonal array with symbol set $\{1,2\}$ and strength 2 [8]:

1	1	1
2	2	1
1	2	2
2	1	2

As observed that four ordered pairs (2-tuples) designed by the rows restricted to the first and third columns, namely $(1,1)$, $(2,1)$, $(1,2)$ and $(2,2)$ are all the possible ordered pairs of the two element set and each appears only single time i.e. once. The second and third columns will give, $(1, 1)$, $(2, 1)$, $(2, 2)$ and $(1, 2)$; again, all possible ordered pairs each appearing once. The same statement

would hold had the first and second columns been used. So this is an orthogonal array of strength of two.

3.1.5 Designing of experiment using Taguchi Method:

The design of an experiment includes the following steps [16]:

- A. Selection of independent variables
- B. Selection of number of level settings for each independent variable
- C. Selection of orthogonal array
- D. Assigning the independent variables to each column
- E. Conducting the experiments
- F. Analyzing the data
- G. Inference

The detail of above steps are given below:

A. Selection of the independent variables:

Before to start conducting an experiment, the knowledge of the product/process under investigation is of prime importance for identifying the factors most likely to influence the outcome. In order to compile a comprehensive list of factors, the input to the experiment is generally obtained from all the persons involved in the process.

B. Deciding the number of levels:

Once the independent variables are selected, the number of levels for each variable is determined. The selection of several levels depends on how much the performance parameters are affected due to different level settings. If the performance parameter is a linear function of the independent variable, then the number of level setting shall be 2. However, if the independent variable is not linearly related, then one can go for 3, 4, or higher levels depending on whether

the relationship is quadratic, cubic or higher order. In the absence of a relationship between the independent variable and the performance parameter, one could choose 2 level settings. After analyzing the experimental data, one can decide whether the assumption of level setting is right or not based on the percent contribution and the error calculations.

C. Selection of an orthogonal array:

Before selecting the orthogonal matrix, the minimum number of experiments to be conducted shall be fixed depending on the total number of degrees of freedom used in the study. The minimum number of experiments that might be run to study the factors should be more than the complete degrees of freedom available. In the measurement of the complete degrees of freedom, the investigator commits one degree of freedom to the overall mean of the response under study. The number of degrees of freedom associated with every factor under study equals one less than the number of levels available for this factor. Hence the total degrees of freedom without interaction effect is more than one. For example, in the case of 11 independent variables, each having two levels, the total degrees of freedom is 12. Hence the selected orthogonal array shall have at least 12 experiments. An L12 orthogonal satisfies this requirement.

D. Assigning the independent variables to columns:

The sequence in which the independent variables are arranged to the vertical column is important. In case of mixed level variables and interaction between variables, the variables are to be assigned at right columns as stipulated by the orthogonal array [16].

Finally, before experimenting, the actual level values of each design variable must be decided. It might be noted that the significance and the percent contribution of the independent variables changes depending on the level values assigned. It is the manufacturer responsibility to set proper level values.

E. Experimenting:

After the orthogonal array is selected, the experiments are performed as per the level combinations. It is required that all the experiments were conducted. The interaction columns and dummy variable columns shall not be considered for operating the experiment, but are needed while analyzing the data to understand the interaction effect. The performance parameter under study is noted down for each experiment to conduct the sensitivity analysis for further.

F. Analysis of the data:

Since each experiment is the combination of multiple factor levels, it is required to segregate the individual effect of independent variables. This can be done by adding up the performance parameter values for the corresponding level settings. For example, in order to find out the main effect of level 1 setting of the independent variable 2, sum the performance parameter values of the experiments 1, 4 and 7. Similarly for level 2, sum the experimental results of 2, 5 and 7 and so on.

Once the mean value of each level of a particular independent variable is calculated, the sum of square of deviation of each of the mean value from the grand mean value is calculated. This sum of square deviation of a particular variable indicates whether the performance parameter is sensitive to the change in level setting. If the sum of square deviation is close to zero or insignificant, one may conclude that the design variables is not influencing the performance of the process. In other words, by conducting the sensitivity analysis, and performing analysis of variance (ANOVA), one can decide which independent factor dominates over other and the percentage contribution of that particular independent variable.

G. Inference:

Table 3.4 shows the 18 experiments corresponding to the L18 orthogonal array with respect to 8 variables

Experiments	P1	P2	P3	P4	P5	P6	P7	P8
1	1	1	1	1	1	1	1	1
2	1	1	2	2	2	2	2	2
3	1	1	3	3	3	3	3	3
4	1	2	1	1	2	2	3	3
5	1	2	2	2	3	3	1	1
6	1	2	3	3	1	1	2	2
7	1	3	1	2	1	3	2	3
8	1	3	2	3	2	1	3	1
9	1	3	3	1	3	2	1	2
10	2	1	1	3	3	2	2	1
11	2	1	2	1	1	3	3	2
12	2	1	3	2	2	1	1	3
13	2	2	1	2	3	1	3	2
14	2	2	2	3	1	2	1	3
15	2	2	3	1	2	3	2	1
16	2	3	1	3	2	3	1	2
17	2	3	2	1	3	1	2	3
18	2	3	3	2	1	2	3	1

From the above mathematical analysis, it is clear that the higher the value of sum of square of an independent variable, the more it has effect on the performance parameter. One can also calculate the ratio of individual sum of square of a particular independent variable to the total sum of squares of all the variables. This ratio gives the percent of the independent variable on the performance parameter [11].

In addition to above, one could find the near optimal solution to the problem. This near optimum value might not be the global optimal solution. However, the solution can be used as an initial / starting value for the standard optimization technique.

3.1.6 Taguchi Implementation on MEMS PMPG:

L₁₈ orthogonal array

L₁₈ orthogonal array was used to find the most control variable affecting the output power generated which has 18 rows equivalent to the number of experiments, with 8 columns corresponding to the number of variables at three levels. L₁₈ OA has 17 DOF calculated as follows (Taguchi 1987), in which 15 were assigned to 8 factors (each one 2 DOF except proof mass material with 1 DOF) and 2 DOF for error. COMSOL Multiphysics version 5 is used for 18 different simulations to find electric energy density (j/m³) at a frequency of 1.2 Hz which is the dominant eigen frequency with respect to z-axis displacement. This simulation is done single time on 60 kg body weight.

$$\text{Degree of Freedom (DOF)} = \text{number of levels} - 1$$

Table 3.5 represents the PMPG parameters level with respect to materials properties.

Level	1	2	3
Proof mass material (P1)	Ni	Cu	Su8
Piezo electric material (P2)	PZT-5A	Gallium Arsenide	PZT-5H
Proof mass length (P3)	3 mm	5 mm	7 mm
Proof mass thickness (P4)	1 mm	2.5 mm	4 mm
Piezo width (P5)	0.12 mm	0.16 mm	0.2 mm
Piezo thickness (P6)	30 um	45 um	60 um
Insulator width (P7)	0.12 mm	0.16 mm	0.2 mm
Insulator thickness (P8)	20 um	30 um	40 um

The table 3.4 indicate about the 18 different simulations performed by choosing 8 variables. The selction of 8 variables are done at three levels. These levels can

Table 3.6 represents the generated electrical energy density with respect to the eigen frequency at all 18 experiments by taguchi L18 orthogonal array.

Experiments	Electric energy density (J/m ³)	First Resonance Frequency (Hz)
1	0.00230	1.09
2	4.4350	1.22
3	0.00618	2.97
4	0.00243	2.91
5	0.03678	1.38
6	0.000923	0.67
7	0.00574	1.98
8	0.00127	0.8
9	0.002636	1.87
10	0.001121	2.93
11	0.02130	2.41
12	0.04321	4.06
13	0.009313	2.67
14	0.00910	4.73
15	0.002123	4.03
16	0.001221	5.06
17	0.00915	2.29

also be increased but the number of experiments would also be increased accordingly.

The selection of three levels are indicated in table 3.5, in which we used three proof mass material Ni, Cu, and SU-8 for level 1, 2, and 3 respectively. The assignment of remaining 7 variable are also done for different materials and dimensions for all three levels.

Table 3.6 indicate the results after 18 simulations done in COMSOL according to experiments mentioned in table 3.4. And it is concluded that the maximum electrical energy density is obtained in experiment 2, which is 4.4350 J/m³ with respect to desired resonance frequency of 1.2 Hz.

3.1.6 Damping in MEMS PMPG device:

Damping is a very important factor in MEMS devices. This plays a very vital role when the structure is hanging device or if air gap is present between the electrodes. Rayleigh damping is used, denotes damping parameters are proportional to the mass α and stiffness β in the following way []:

$$Q = \frac{\text{Output displacement}}{\text{Input displacement}}$$

$$\varepsilon = \frac{1}{2Q} \quad (12)$$

$$\alpha = \frac{\omega_1}{\omega_2} \quad (13)$$

$$\alpha = 2\omega_1\omega_2 \quad (14)$$

$$\beta = 2b \quad (15)$$

where ω_1, ω_2 are first and second angular frequency (rad/s). ζ is the damping coefficient. Q is the quality factor.

3.1.7 Squeeze film damping:

For MEMS devices with a plate that moves against a trapped film, squeeze film air damping has been a problem of great importance as the mechanism dominates the damping and thus substantially affects the system frequency response [11]. The dynamic behaviour of various MEMS devices such as accelerometers, gyroscopes, energy harvesters optical switches, micro-mirrors etc. is significantly affected by the squeeze film air damping of the mechanical structures.

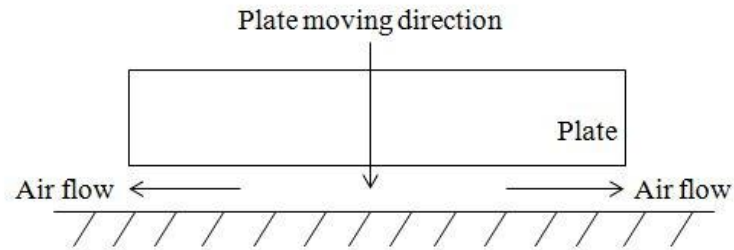


Fig 3.6 shows the squeeze film damping air flow.

Finally, squeeze film damping coefficient for rectangular plate can be calculated by [12]

$$c_{plate} = \frac{\mu_{eff} l w^3}{h_0^3} \beta\left(\frac{w}{l}\right) \quad (16)$$

where w is width of the plate, l is length of the plate and factor $\beta(w/l)$ is

$$\beta\left(\frac{w}{l}\right) = \left\{ 1 - \frac{192}{\pi^5} \left(\frac{w}{l}\right) \sum_{n=1,3,5}^{\infty} \frac{1}{n^5} \tanh\left(\frac{n\pi l}{2w}\right) \right\} \quad (17)$$

All dimesions used here according to table 3.2 for nickel proof mass.

3.1.8 Slide film damping:

For MEMS devices with a plate that moves in parallel with their surfaces, the slide film air damping has been a problem of great importance as it plays a major role in the energy dissipation of the dynamic system. The dynamic behaviour of various surface micromachined devices such as resonators, actuators, accelerometers, gyroscopes etc. is significantly affected by the slide film air damping of the mechanical structures [12].

Slide film damping occurs when two plates of an area A , separated by a distance d , slide parallel to each other as shown in Fig 3.7 The relative motion of the parallel structures invokes a fluid flow that exerts a force opposing the relative motion.

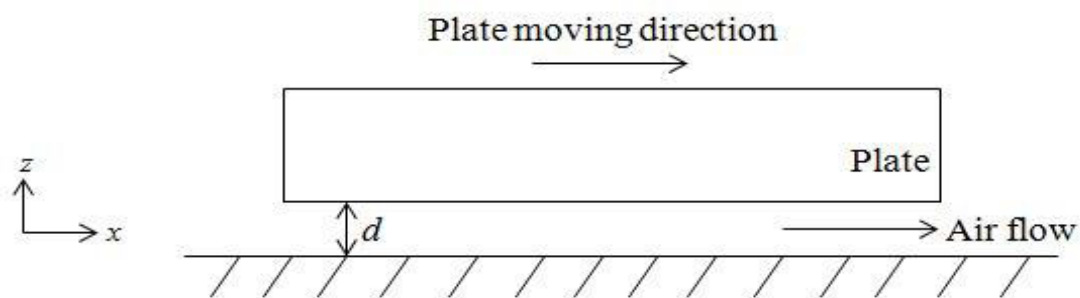


Fig 3.7 shows the slide film damping air flow.

The damping coefficient of slide film damping is defined as :

$$C_{plate} = \frac{\tau}{v_x} = \frac{\mu_{eff} A}{d} \quad (18)$$

All dimensions used here according to table 3.2 for nickel proof mass.

3.1.9 Torsional damping:

For torsion micro-structure devices which operate at atmospheric pressure, squeeze film damping is very dominant damping phenomenon and this may be due to the flow of air around the structure or squeezing of air in gap between a rotating structure and a fixed substrate [11]. When the movable plate rotates about the rotation axis, the air is squeezed underneath the plate, in the small gap between the tilting movable plate and substrate, and the squeeze film damping phenomenon occurs as shown in figure 3.8.

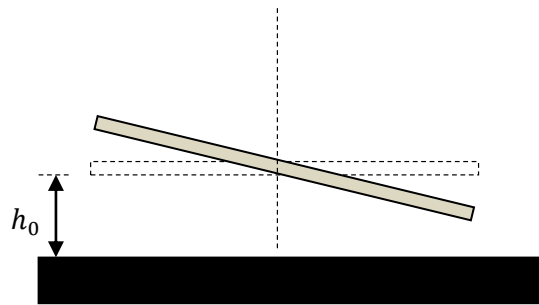


Fig 3.8 shows the torsional film damping air flow.

The squeeze film damping torque comes from the pressure distribution on the plate surface. Various representations of the infinite second order series is used to find out the coefficient of damping in torsion micro-structures. These expressions are derived by using a nonlinear isothermal Reynold's equation as a model for pressure distribution in squeeze film [15].

So the damping coefficient for the torsional micro-structures is given as [2]:

$$C = \frac{48}{\pi^6(b^2+4)} \frac{\mu w_m l_m^5}{h_0^3} \quad (19)$$

Where, $b = \frac{l_m}{w_m}$ and w_m is the width of the plate.

All dimesions used here according to table 3.2 for nickel proof mass.

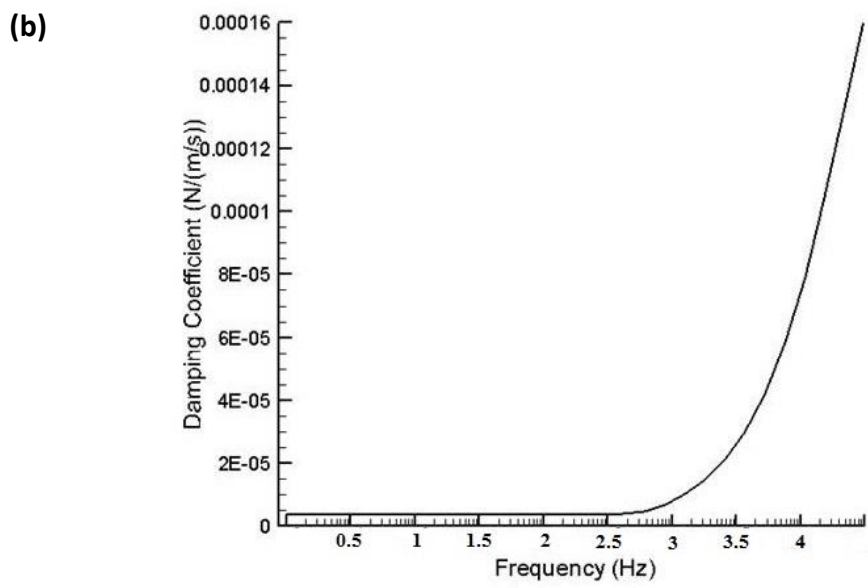
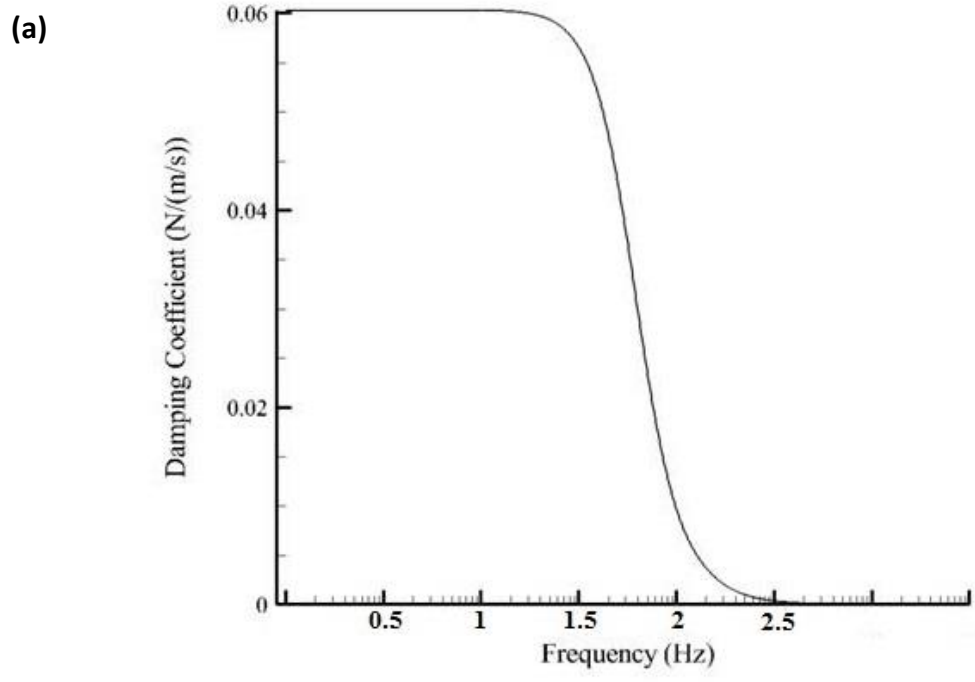


Fig. 3.9 Represents the damping coefficient of squeeze film damping, and (b) shows the damping coefficient of slide film damping at 1.2 Hz frequency [13].

Table 3.7 damping coefficient of squeeze and slide film damping [13].

	Damping Coefficient (Analytical)	Damping Coefficient (Simulation)
Squeeze film damping	5.84×10^{-2}	6.04×10^{-2}
Slide film damping	3.58×10^{-6}	3.62×10^{-6}

The above figures and table indicates the damping coefficient and frequency graph for both squeeze and slide film damping at frequency range of 0-2.5 Hz. The damping coefficient value is also verified by mathematically by using the equation 16 and 18. The analytical value are found to 5.84×10^{-2} and 3.58×10^{-6} which are very close to the simulated value as shown in table 3.7.

Chapter 4

DEPOSITION AND CHARACTERIZATION

4.1: Elctro-depostion of Cu and Ni:

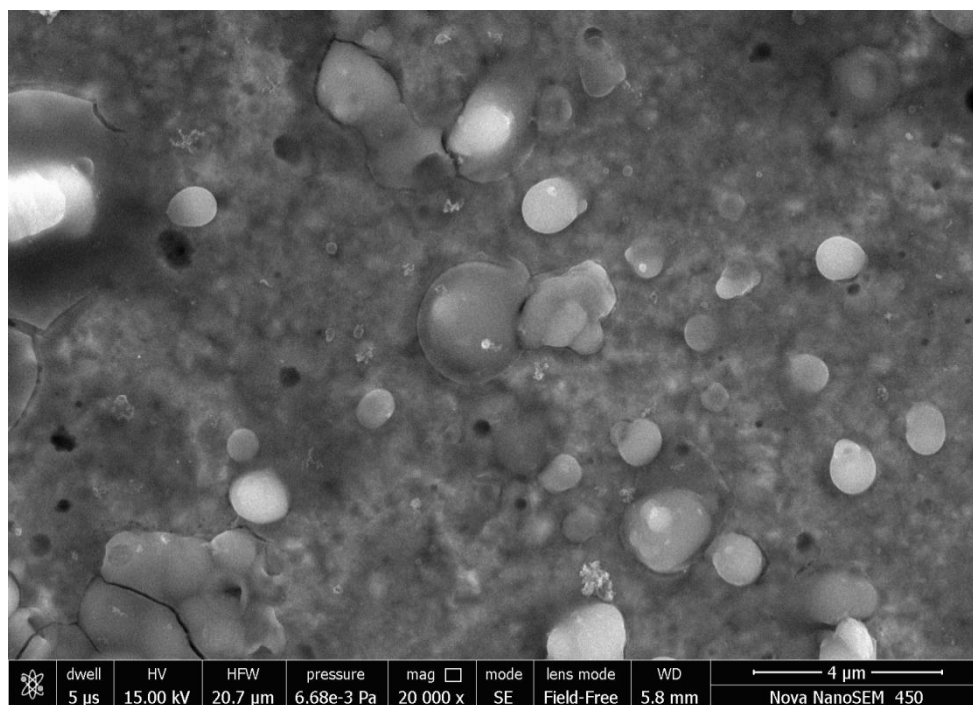
A surface characterization is performed to view the surface morphology to select an optimal proof mass which is responsible for the low eigen frequency. Here we did an experimental study on two materials: copper and nickel, which are giving a nearby resonance frequency of 1.2 Hz.

Electroplating of Cu and Ni are done to analyze the best morphology for proof mass at low frequency. The commercially available solutions copper sulfate and nickel sulphamate are used to prepare a bath of electroforming and deposition of copper and nickel, respectively. A constant current density is used for deposition, and temperature range is varied between 30 to 60 degree C for stress-free deposition. A Teflon setup with electrode separation of 9 cm is prepared for electrode position. For copper electrode position; a small copper plate, whereas a pure nickel plate is used for nickel deposition at one end of the setup to make it anode. A SSP (single side polished) oxidized silicon substrate is used and Titanium (Ti) and Gold (Au) is deposited as seed layers containing thickness of 200 and 2000 Å respectively by RF sputtering to create a conductive layer for electrode position. A Ti layer is used to provide a good adhesion for the Au seed layer which is confirmed by Atomic Force Microscopy (AFM) by measuring roughness of gold layer as 20 nm.

Both deposition rate and morphology depend upon the current density. We used current density 8 mA/cm² for both deposition and morphological characterization is done by AFM and FESEM.

4.2: Charcaterization of deposited Cu and Ni thin films:

(a)



(b)

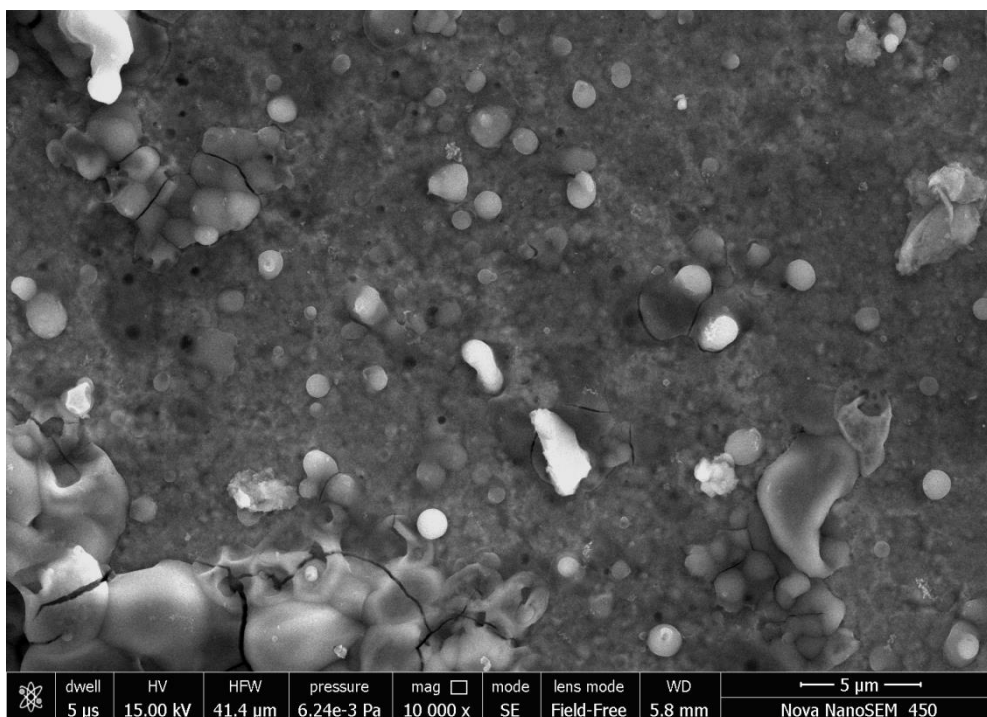
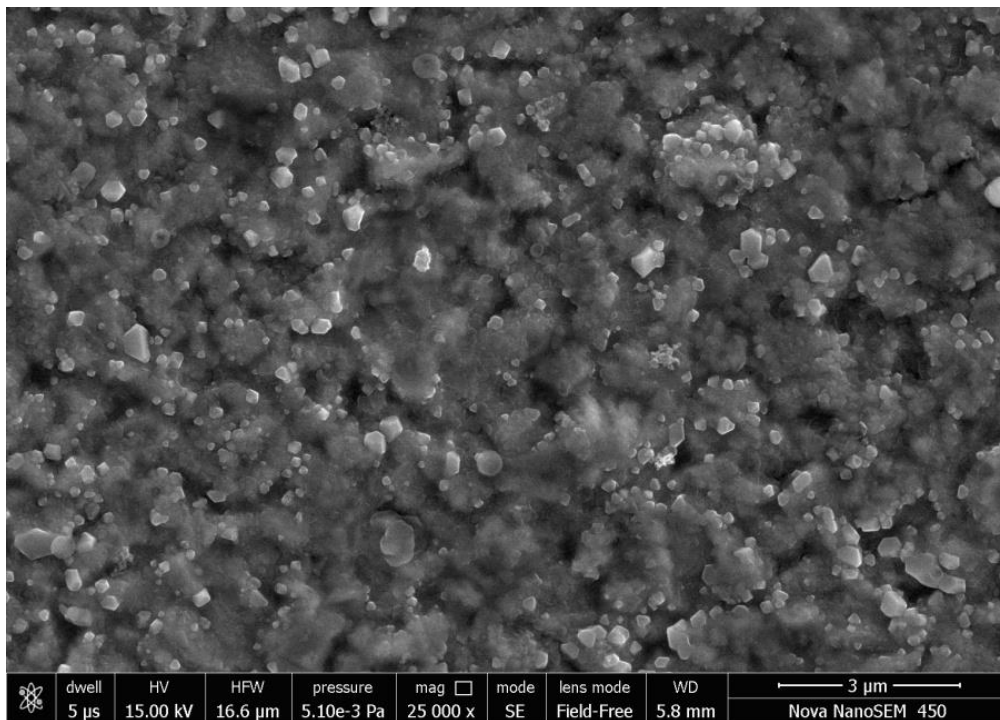


Fig. 4.1 (a), and (b) shows the FESEM images of electroplated Ni material on Si substrate .

(a)



(b)

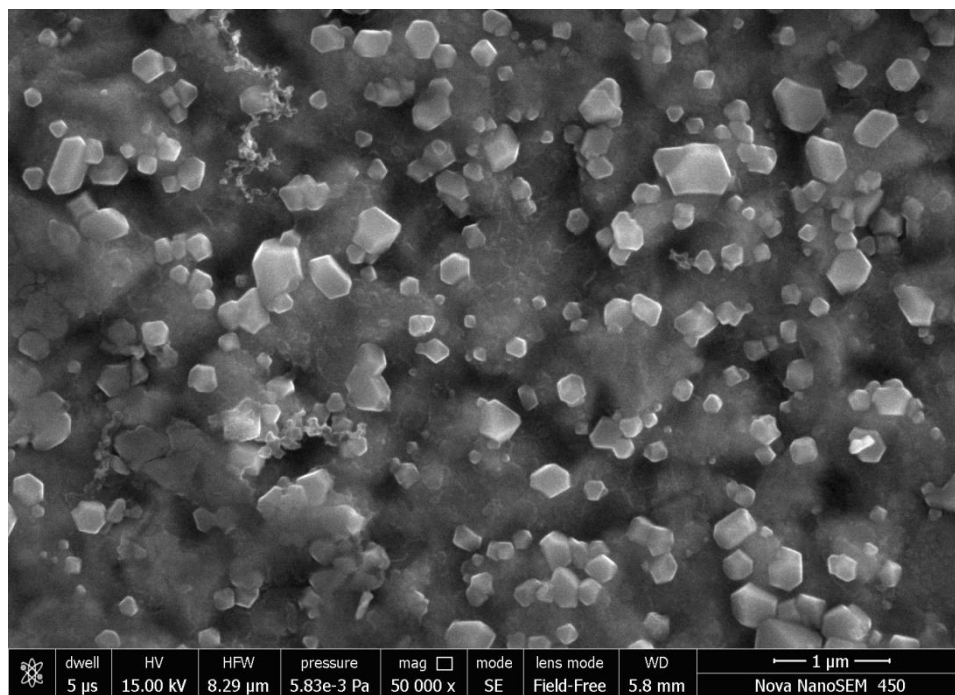
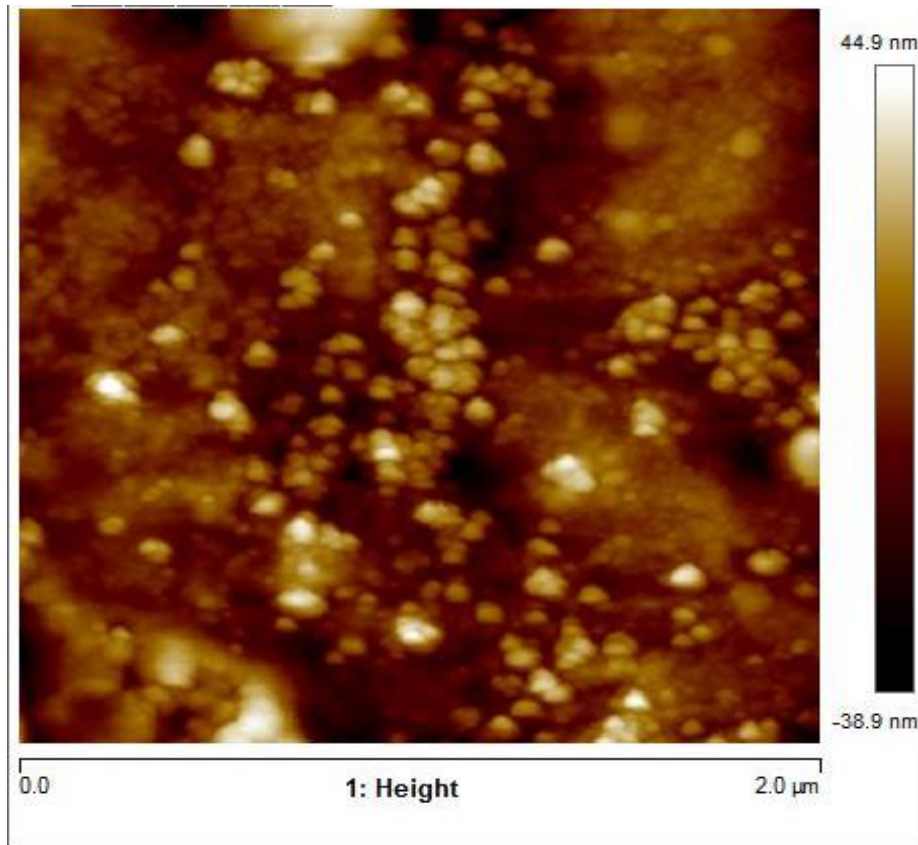


Fig. 4.2 (a) and (b) shows the FESEM images of Cu electroplating at 25000 and 50000 magnification respectively.

(a)



(b)

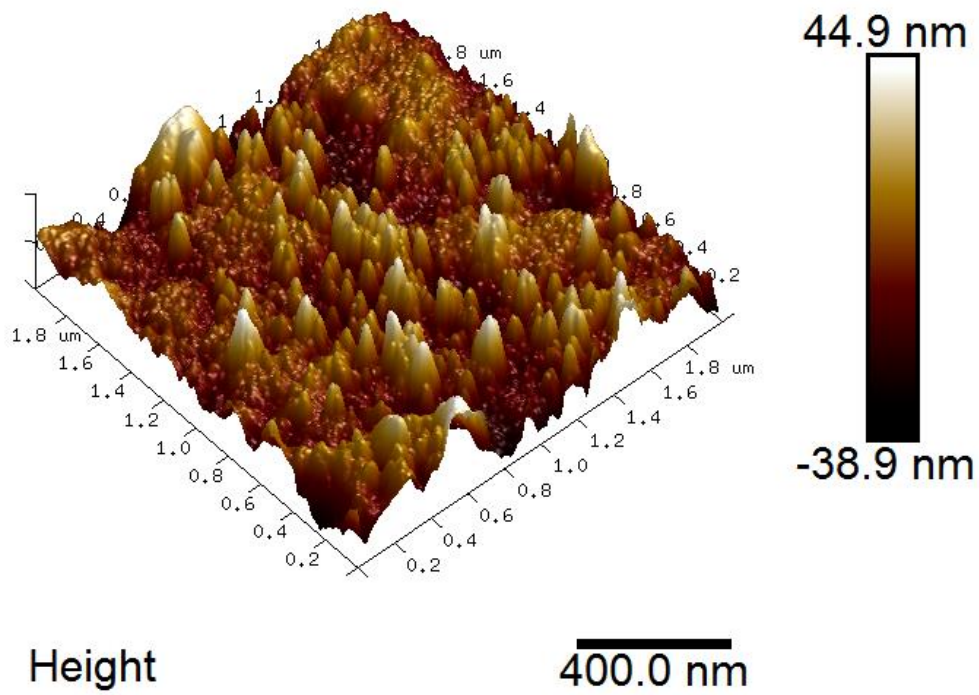
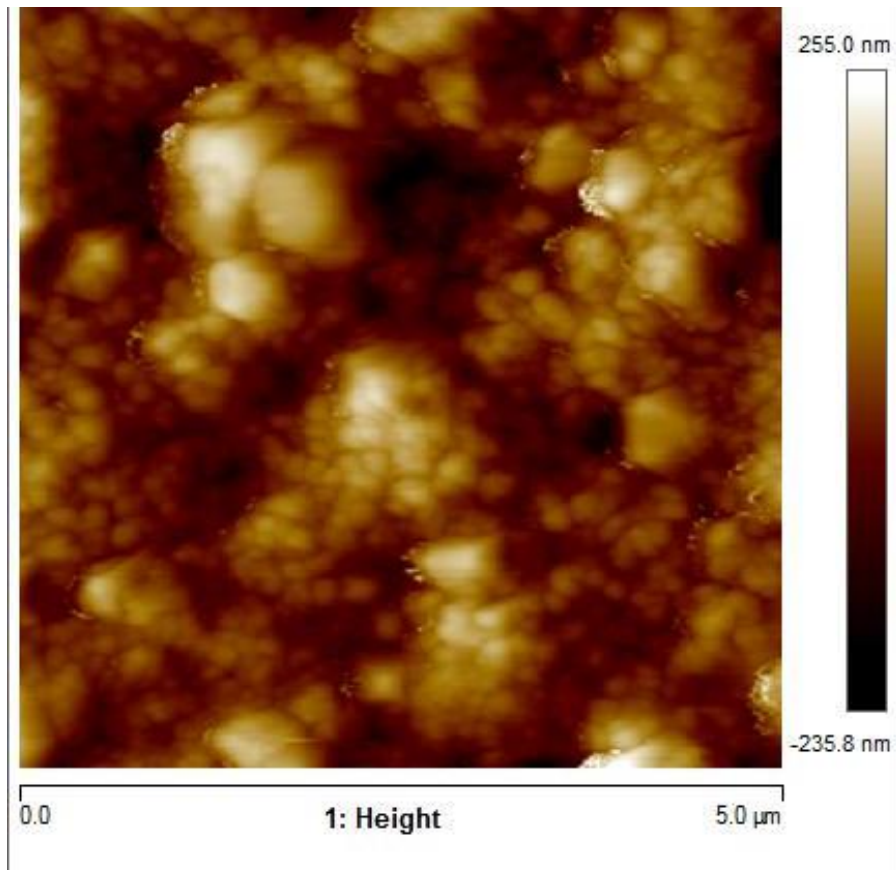


Fig 4.3 (a) and (b) shows the AFM 2D and 3D images respectively of electroplated Ni at 2 μm scale.

(a)



(b)

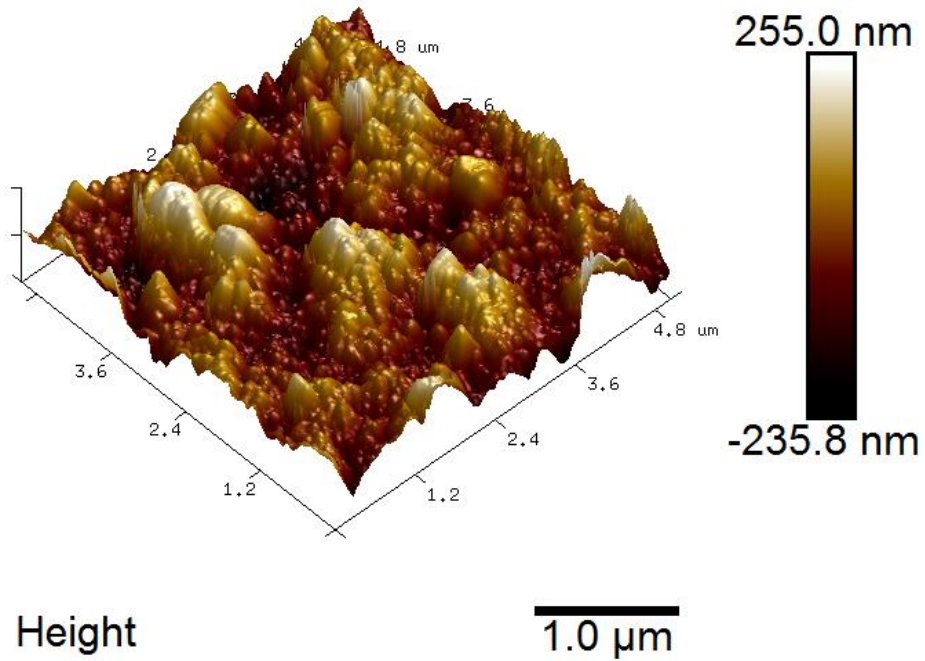
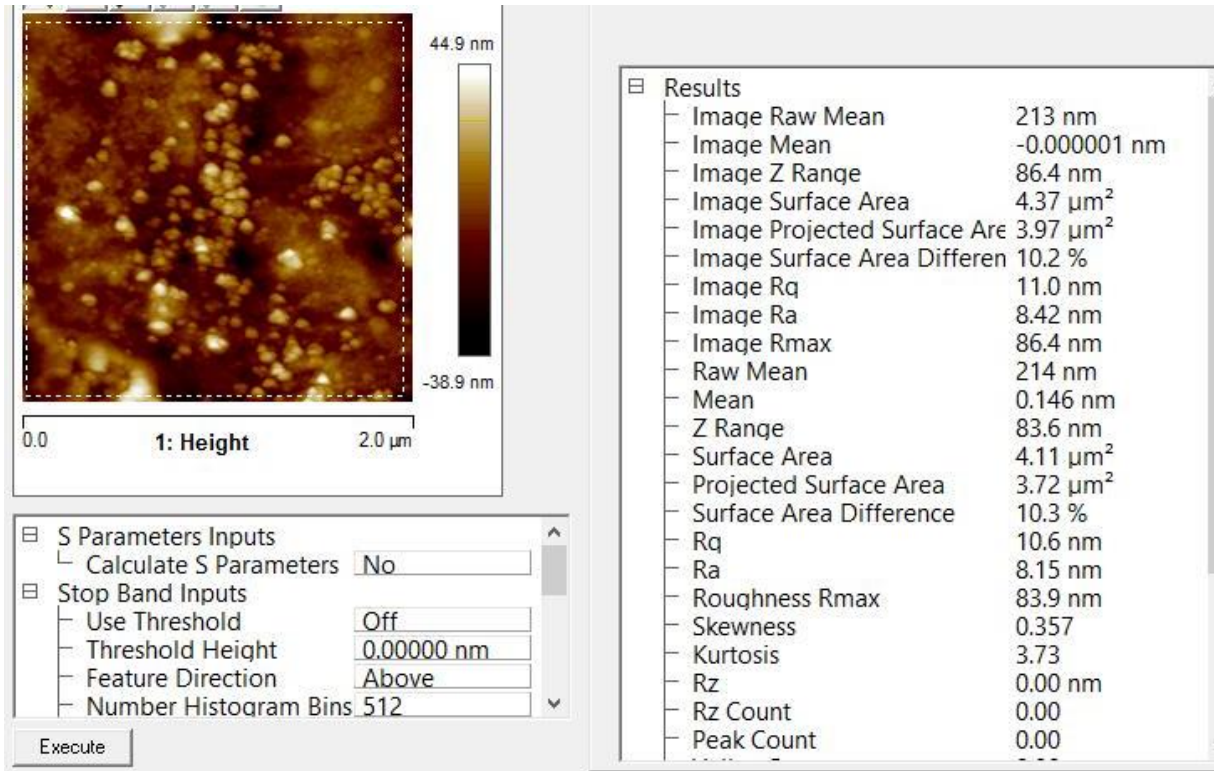


Fig 4.4 (a), and (b) represents the AFM image of 2D and 3D respectively of electrodeposited Cu at 5μm scale.

(a)



(b)

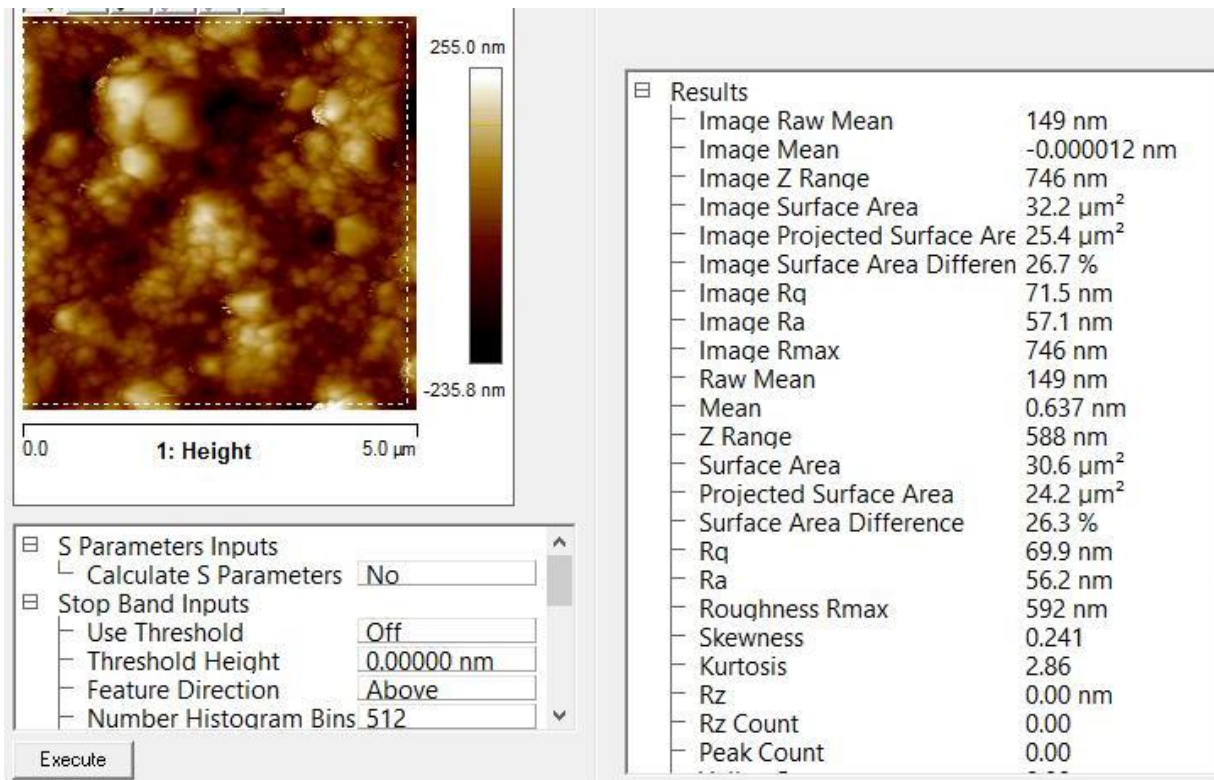


Fig. 4.5 (a) represents the roughness of electroplated Ni is $R_{max} = 86.4$ nm, while (b) shows the roughness of electroplated Cu is $R_{max} = 746$ nm

The Bruker multimode 8 Atomic Force Microscopy (AFM) in tapping mode is used to identify the morphology of deposited Cu and Ni surface. 2D and 3D height and phase images of AFM confirm that Cu deposition has some kind of porous and asymmetric shape structure with very high roughness of 746 nm, whereas Ni has a circular shaped structure with very dominant roughness of 86.4 nm. This porosity and shape is also confirmed by Field Emission Scanning Electron Microscope (FESEM). A Nova NanoSEM 450 is used to clarify the morphology picture of both deposited films. FESEM images of Ni shows that the distribution of particle is in circular and ball shape structure which makes it suitable for proof mass choice while the Cu deposition indicates porosity and non-uniformity in the structure which makes it unsuitable for proof mass layer.

Chapter -5

CONCLUSION AND FUTURE WORK

In this thesis, detail study of MEMS piezoelectric micro power generator for cardiac pacemaker has been done. Simulation is performed in COMSOL multiphysics tool to do the eigen frequency analysis, frequency domain analysis. The bridge type cantilever structure is used over other types of cantilever as it has advantage that total mass of the structure is increased and we are able to achieve the lower resonance frequency of 1.2 Hz. One of the most important factor damping is also measured with the help of coventor ware software. In the designed PMPG, the squeeze film damping is very dominant due to z-axis motion. Both squeeze film and slide film damping simulation results are compared with analytical results. Both results match closely.

Taguchi method is used to achieve the optimum design parameters for MEMS PMPG cardiac pacemaker. L₁₈ orthogonal array design of taguchi is performed by doing 18 different simulations in COMSOL 5. The resultant current, voltage, electric potential, energy density and power are extracted from simulation results.

To find the precise choice of proof mass, an experiment is done by depositing the copper and nickel layer on silicon substrate by electro deposition. Both deposition were characterized by Atomic Force Microscopy (AFM), and Field Emission scanning Electron Microscope (FESEM). The AFM results provide the information about roughness of both deposited films and also an idea about morphological changes as porosity while the FESEM results provide the high resolution view of deposited films by which the best morphology of film is concluded.

In future, This PMPG structure can also be simulated by Coventore ware and we can verify the simulation results with COMSOL multiphysics. Second, We can fabricate the proposed structure and can characterize for measurement of electric potential, stored energy and frequency response. Furthur, different dimensions/structures of PMPG can be explored for 1.2 Hz frequency.

REFERENCES

- [1] Mohd H.S. Alrashdan, Azrul Azlan Hamzah, Burhanuddin Yeop Majlis (2015) Design and optimization of cantilever based piezoelectric micro power generator for cardiac pacemaker. *Microsystem Technol* 21:1607-1617, DOI 10.1007/s00542-014-2334-1.
- [2] Jong Cheol, Jae Yeong Park, Yoon-Pyo Lee (2010) Modeling and characterization of piezoelectric D_{33} – mode MEMS energy harvester. *Journal of Microelectromechanical Systems*, Vol. 19, No. 5.
- [3] Salem Saadon, and Othman Sidek (2014) E- Shaped cantilever based MEMS piezoelectric energy harvester for low frequency applications. *Journal of Optoelectronics and Advanced Materials*.
- [4] Hitesh Kumar Sharma, Ankush Jain, Ram Gopal. Estimation of slide film damping in laterally moving micro-structures using FEM simulations. V-IMPACT, 27-28 February, 2014 , India
- [5] Ankush jain, Hitesh Kumar Sharma, Ram Gopal (2015) New architecture of torsional gyroscope having robust sense mode. *Journal of Micro/Nanolithography, MEMS, and MOEMS (JM3) (SPIE)*.
- [6] M. Bao and H. Yang, “Squeeze film air damping in MEMS,” *Sensors and Actuators A: Physical*, vol. 136, no. 1, pp. 3-27, May 2007.
- [7] M. Bao, *Analysis and Design Principles of MEMS Devices*, 1st ed., vol. 2. Elsevier: Clarendon, 2005, pp. 115-174.
- [8] T. Veijola, H. Kuisma, J. Lahdenpera, and T. Ryhanen, “Equivalent-circuit model of the squeezed gas film in a silicon accelerometer,” *Sensors and Actuators A: Physical*, vol. 48, pp. 239-248, May 1995.

- [9] A.K.Pandey, R. Pratap, F.S. Chau, Effect of pressure on fluid damping in MEMS torsional resonators with flow ranging from continuum to molecular regime. *Society for Experimental Mechanics* 48:91-106 (2008).
- [10]Hamid Moeenfard, Mohammad Taghi Ahmadian, Anooshiravan Farshidianfar, Modelling squeezed film air damping in torsional micromirrors using extended Kantorovich method. *Springer Meccanica* 48:791-805 (2013).
- [11]Feixia Pan, Joel Kubby, Eric Peeters, Alex T Tran and Subrata Mukherjee, Squeeze film damping effect on the dynamic response of a MEMS torsion mirror. *J.Micromech. Microeng.* 8 200-208 (1998).
- [12]Martin Gugat, Efficient numerical evaluation of semi-analytical models for squeeze film damping for torsion mirrors. *Journal of Nanomechanics and micromechanics*, 10.1061/(ASCE) NM.2153-5477.0000075 (2013).
- [13]Coventor Ware ANALYZER, Version 2012, Reference: Extended Capabilities.
- [14]COMSOL Multiphysics Tool, Version-5, Reference: Extended capabilities.
- [15]A newsletter published by American Heart Association, heart.org/answerbyheart.
- [16]Introduction to taguchi method, “Chapter-2”, www.ecs.umass.edu/mie/labs/mda/fea/sankar/chap2.